12

Plane four-node elements with drilling rotation

The drilling rotation, as a degree of freedom, is particularly important for shell elements, but the 2D elements with drilling rotations are much simpler and, hence, very useful in developing and testing specific ways of incorporating the drilling rotation terms. We designate the 2D elements with drilling rotations as "2D+drill".

The drilling rotation is defined as the rotation vector normal to the tangent plane of the element. However, for 2D elements, the normal direction is defined by one vector $\mathbf{t}_3$, normal to the plane of element, so it suffices to consider the angle of drilling rotation, ω. The nodal drilling rotations of a 2D+drill element are shown in Fig. 12.1.

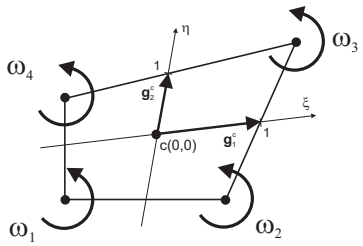

Fig. 12.1 Nodal drilling rotation angles $\omega_I\,(I = 1, 2, 3, 4)$ of plane four-node element.

The drilling rotation can be incorporated into the 2D+drill elements, and shell elements as well, in two ways:

1. Using the so-called Allman shape functions which approximate the element's displacements in terms of nodal displacements $\mathbf{u}_I$ and nodal drilling rotations ω_I. The classical approach based on Allman

shape functions uses the potential energy functional and is valid only for small drilling rotations. The generalized version, valid for finite rotations, is described in Sect. 12.7.

2. Using bilinear shape functions and the drill RC equation, which is extracted from the RC equation, $\text{skew}(\mathbf{Q}^T\mathbf{F}) = \mathbf{0}$, as discussed in detail in Sect. 3. This equation can be implemented in a finite element in several ways, see Sect. 12.3. Some of them use the weak forms, and correspond to the 3D mixed functionals incorporating rotations of Sect. 4. The drill RC for shells was derived in Sect. 6.2. The 2D+drill elements based on bilinear shape functions are described in Sect. 12.6.

Chronologically, the approach based on the Allman shape functions was first, but tests indicate that the elements based on the drill RC equation perform slightly better.

Crucial for a good performance of 2D+drill elements is the use of EADG enhancement, which also affects the RC equation and, for this reason, is more suitable than the EAS enhancement. The EADG method was discussed in Sect. 11.4.3; its extension to formulations with rotations is given in Sect. 12.4.

All the four-node elements described in sequel are developed for finite (unrestricted) drilling rotations.

12.1 Basic relations for drill RC equation

Drill RC for shells. In the RC of eq. (3.8), we neglect the terms which do not depend on the drilling rotation. Then, only the components 12 and 21 of this equation remain and we denote $\left[\text{skew}(\mathbf{Q}^T\mathbf{F})\right]_{12} \doteq r_\omega$, where

$$r_\omega \doteq \tfrac{1}{2}(\mathbf{x}_{0,1}\cdot\mathbf{a}_2 - \mathbf{x}_{0,2}\cdot\mathbf{a}_1) \tag{12.1}$$

or, in terms of tangent displacement components u, v and the drilling rotation ω,

$$2r_\omega \doteq -(v_{,2} + u_{,1} + 2)\,\sin\omega + (v_{,1} - u_{,2})\,\cos\omega. \tag{12.2}$$

In this way, the tensorial RC, $\text{skew}(\mathbf{Q}^T\mathbf{F}) = \mathbf{0}$, is reduced to the scalar drill RC, $r_\omega = 0$.

Three forms of drill RC for 2D problem. We can obtain an alternative but equivalent form of the drill RC equation considering a 2D problem, for which we have

$$\mathbf{F} = \begin{bmatrix} F_{11} & F_{12} \\ F_{21} & F_{22} \end{bmatrix}, \qquad \mathbf{Q} = \begin{bmatrix} \cos\omega & -\sin\omega \\ \sin\omega & \cos\omega \end{bmatrix}, \tag{12.3}$$

where ω is the drilling rotation angle, and we obtain

$$\operatorname{skew}(\mathbf{Q}^T\mathbf{F}) = \begin{bmatrix} 0 & -r_\omega \\ r_\omega & 0 \end{bmatrix}, \tag{12.4}$$

where $r_\omega \doteq \frac{1}{2}(A\sin\omega + B\cos\omega)$, $A \doteq F_{11} + F_{22} = u_{1,1} + u_{2,2} + 2$, and $B \doteq F_{12} - F_{21} = u_{1,2} - u_{2,1}$. Hence, the RC equation, $\operatorname{skew}(\mathbf{Q}^T\mathbf{F}) = \mathbf{0}$, is reduced to one scalar equation,

$$r_\omega \doteq \tfrac{1}{2}(A\sin\omega + B\cos\omega) = 0. \tag{12.5}$$

Using this equation, we can formulate the constraint for the drilling rotation in one of the following forms:

1. For rotations $|\omega| < \pi/2$, we can divide eq. (12.5) by $\cos\omega$ to obtain

   $$\omega^* = -\arctan\frac{B}{A}. \tag{12.6}$$

   Hence, the first form of the drill RC is defined as

   $$c \doteq \omega - \omega^* = 0. \tag{12.7}$$

2. For large rotations, the constraint can be written for an increment. For $\omega \doteq \omega_n + \Delta\omega^*$, using trigonometric identities, we obtain

   $$\sin\omega = s_n\cos\Delta\omega^* + c_n\sin\Delta\omega^*, \qquad \cos\omega = c_n\cos\Delta\omega^* - s_n\sin\Delta\omega^*,$$

   where $s_n \doteq \sin\omega_n$ and $c_n \doteq \cos\omega_n$. For $|\Delta\omega^*| < \pi/2$, we can divide by $\cos\Delta\omega^*$ and, from eq. (12.5), we obtain

   $$\Delta\omega^* = -\arctan\frac{As_n + Bc_n}{Ac_n - Bs_n}. \tag{12.8}$$

   Hence, the second form of the drill RC is defined as

   $$c \doteq \Delta\omega - \Delta\omega^* = 0. \tag{12.9}$$

3. We can directly use eq. (12.5) for large rotations and define the third form of the drill RC as follows:

   $$c \doteq r_\omega = \tfrac{1}{2}\left(A\sin\omega + B\cos\omega\right) = 0, \tag{12.10}$$

   where A and B depend on $\mathbf{u}$. This form of the drill constraint can be linearized using symbolic differentiation.

Rotational invariance of drill RC equation for 2D problems. Consider components of displacement and rotation tensors in the reference Cartesian basis $\{\mathbf{i}_k\}$.

Let a 2D body be located in the $\{\mathbf{i}_1, \mathbf{i}_2\}$-plane and its deformation, except for the thickness change, also takes place in this plane. The orientation of the local ortho-normal basis $\{\mathbf{t}_k\}$ is defined by the rotation tensor $\mathbf{R}$, i.e. $\mathbf{t}_k = \mathbf{R}\,\mathbf{i}_k$. The normal vector $\mathbf{t}_3$ coincides with $\mathbf{i}_3$. For $\mathbf{Q}$ and $\mathbf{F}$, we use the representations of eq. (12.3) and, additionally, we define

$$\mathbf{R} \doteq \begin{bmatrix} \cos\alpha & -\sin\alpha \\ \sin\alpha & \cos\alpha \end{bmatrix}. \tag{12.11}$$

Define the following back-rotated matrices:

$$\mathbf{Q}_* \doteq \mathbf{R}^T\mathbf{Q}\,\mathbf{R}, \qquad \mathbf{F}_* \doteq \mathbf{R}^T\mathbf{F}\,\mathbf{R}, \qquad (\mathbf{Q}^T\mathbf{F})_* \doteq \mathbf{R}^T(\mathbf{Q}^T\mathbf{F})\,\mathbf{R}, \tag{12.12}$$

where $(\,\cdot\,)_*$ designates a back-rotated object. We can check that $\mathbf{Q}_*^T\mathbf{F}_* = (\mathbf{Q}^T\mathbf{F})_*$ and that

$$\operatorname{skew}(\mathbf{Q}_*^T\mathbf{F}_*) = \operatorname{skew}(\mathbf{Q}^T\mathbf{F})_* = \operatorname{skew}(\mathbf{Q}^T\mathbf{F}). \tag{12.13}$$

As a consequence, in the local basis $\{\mathbf{t}_k\}$, we can use the drill RC equation in terms of components in the global basis $\{\mathbf{i}_k\}$.

Remark. The above property does not hold for 3D problems, for which $\mathbf{F}$, $\mathbf{Q}$, and $\mathbf{R}$ are 3×3 matrices. We checked this for the canonical parametrization of the rotation tensor. For 3D problems, only the property $\mathbf{Q}_*^T\mathbf{F}_* = (\mathbf{Q}^T\mathbf{F})_*$ holds and, hence, only

$$\operatorname{skew}(\mathbf{Q}_*^T\mathbf{F}_*) = \operatorname{skew}(\mathbf{Q}^T\mathbf{F})_* \tag{12.14}$$

can be used in the implementation of the element.

Calculation of drilling rotation for given displacement. Calculation of the drilling rotation for the given displacement $\mathbf{u}$ is a post-processing operation, but is not trivial because the equation involved is non-linear w.r.t. drilling rotation angle.

Assume that the displacement $\mathbf{u}$ is given and we wish to calculate the drilling rotation, ω. The above-defined three forms of the drill RC can be used as follows:

M1. Equation (12.6) is used, so the rotation is restricted, i.e. $\omega < |\pi/2|$.

M2. Equation (12.8) is used with the update formula $\omega = \omega_n + \Delta\omega$, where ω_n is known. Besides, A and B depend on the known $\mathbf{u}$. No iterations are needed. The increment is restricted, i.e. $\Delta\omega < |\pi/2|$, but the total rotation ω is not.

M3. Equation (12.10) is used with the Newton method,

$$\Delta\omega = -r_\omega / r_{\omega,\omega}, \qquad \omega = \omega_n + \Delta\omega. \tag{12.15}$$

Iterations are needed. Formally, $\Delta\omega$ is not restricted but the radius of convergence of the Newton method is.

Summarizing, M2 and M3 are incremental and can be used to obtain arbitrarily large drilling rotations.

Example. Drilling rotation for rigid body rotation. The above defined methods can be compared for a rigid rotation of a body, for which

$$\mathbf{F} \doteq \frac{\partial \mathbf{x}}{\partial \mathbf{y}} = \begin{bmatrix} \cos\alpha & -\sin\alpha \\ \sin\alpha & \cos\alpha \end{bmatrix}, \tag{12.16}$$

where α is the angle of a rigid rotation. Then, $A \doteq F_{11} + F_{22} = 2\cos\alpha$ and $B \doteq F_{12} - F_{21} = -2\sin\alpha$ (see the definitions following eq. (12.4)), and we can calculate ω for increasing values of α using the methods defined above. The solutions are shown in Fig. 12.2. The solutions by

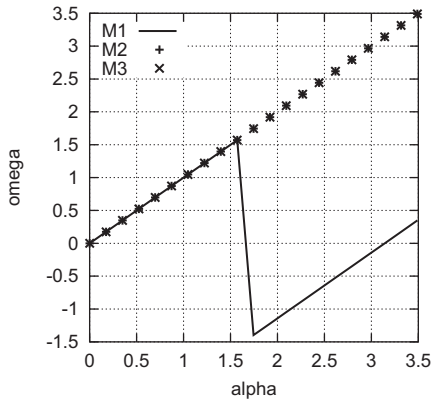

Fig. 12.2 Drilling rotation calculated by three formulas. $\Delta\alpha = 10^{\circ}$.

M2 and M3 coincide; they are unrestricted and $\omega = \alpha$, as required. The solution by M1 is restricted, i.e. $\omega < |\pi/2|$.

The solutions were obtained for $\Delta\alpha = 10^{\circ}$, but larger steps were also tested. M2 performs correctly for up to $\Delta\alpha = 89^{\circ}$, due to the restricted domain of arctan, while M3 for up to $\Delta\alpha = 69^{\circ}$; for larger steps, it converges to some shifted (incorrect) values.

Note that even $\Delta\alpha = 69^{\circ}$ is above the capabilities of current algorithms, e.g. the energy and momentum conserving algorithm ALGO-C1 for rotational rigid body dynamics can perform similar steps, but then the accuracy is poor, see Sect. 9.4.3.

12.2 Difficulties in approximation of drill RC

Approximation of drilling rotation. The drilling rotation is approximated by the bilinear shape functions $N_I(\xi,\eta)$ of eq. (10.3) as follows:

$$\omega(\xi,\eta) = \sum_{I=1}^{4} N_I(\xi,\eta)\ \omega_I, \tag{12.17}$$

where ω_I are the drilling rotations at the corner nodes, see Fig. 12.1, and the natural coordinates $\xi,\eta \in [-1,+1]$. Hence, the drilling rotation is analogously approximated as displacements, see eq. (10.7).

Difficulties in approximation of the drill RC equation. For the equal-order bilinear the approximations of displacements and the drilling rotation, the drill RC equation of the four-node element is incorrectly approximated.

To illustrate the problem, we consider a 2×2 square element with the center located at the origin of the Cartesian coordinate system. Then the Cartesian coordinates are equal to the natural coordinates, i.e. $x = \xi$ and $y = \eta$, and the Jacobian matrix is an identity matrix.

The bilinear approximation functions for displacements and drilling rotations can be written as

$$u(\xi,\eta) = u_0 + u_1\,\xi + u_2\,\eta + u_3\,\xi\eta, \qquad v(\xi,\eta) = v_0 + v_1\,\xi + v_2\,\eta + v_3\,\xi\eta,$$

$$\omega(\xi,\eta) = \omega_0 + \omega_1\,\xi + \omega_2\,\eta + \omega_3\,\xi\eta, \tag{12.18}$$

where $u_i,\, v_i,\, \omega_i \quad (i = 0,\ldots,3)$ are functions of nodal values of the respective components. We consider the linearized form of the drill RC of eq. (12.10), i.e.

$$c \doteq \omega + \frac{1}{2}(u_{,\eta} - v_{,\xi}) = 0, \tag{12.19}$$

where $u_{,\eta} = u_{1,2}$ and $v_{,\xi} = u_{2,1}$. Using the above approximation functions, grouping the terms, we obtain

$$\left[\omega_0 + \frac{1}{2}(u_2 - v_1)\right] + \left(\omega_1 + \frac{1}{2}u_3\right)\xi + \left(\omega_2 - \frac{1}{2}v_3\right)\eta + \underline{\underline{\omega_3\,\xi\eta}} = 0. \quad (12.20)$$

The constant and linear terms do link the displacement and rotational parameters, indeed, but the bilinear (underlined) term contains only the rotational parameter ω_3. This last term may lead to wrong solutions in certain situations for the reason explained below.

Let us rewrite the constraint in the form $c(\xi,\eta) \doteq c_0 + c_1\xi + c_2\eta + \omega_3\xi\eta$. If we use the penalty method, then the weak form of this constraint is

$$\frac{1}{2}\int_{-1}^{+1}\int_{-1}^{+1} c(\xi,\eta)^2\ \mathrm{d}\xi\mathrm{d}\eta = 2c_0^2 + \frac{2}{3}(c_1^2 + c_2^2) + \underline{\underline{\frac{2}{9}\omega_3^2}}, \quad (12.21)$$

i.e. ω_3 does not vanish upon integration. As a consequence, the penalty method enforces the condition $\omega_3 = 0$ which, generally, is incorrect and can yield an over-stiffened solution.

To alleviate this problem, we remove the bilinear term from eq. (12.20), and use the equation which is only linear in ξ and η, i.e.

$$\left[\omega_0 + \frac{1}{2}(u_2 - v_1)\right] + \left(\omega_1 + \frac{1}{2}u_3\right)\xi + \left(\omega_2 - \frac{1}{2}v_3\right)\eta = 0. \quad (12.22)$$

In a symbolic derivation of an element, the bilinear term can be removed in one of the following ways:

1. Using the linear expansion of eq. (12.20) at the element's center,

$$c(\xi,\eta) \doteq c_c + \xi(c_{,\xi})_c + \eta(c_{,\eta})_c, \quad (12.23)$$

   where the subscript c denotes the element's center, see also eq. (12.28).
2. Evaluating this equation at the mid-points of the element's edges,

$$(\xi,\eta) = (0,\pm 1), \qquad (\xi,\eta) = (\pm 1, 0), \quad (12.24)$$

   where either ξ or η is zero, so the bilinear term in eq. (12.20) is always zero.

The lack of an equation for ω_3 means that the tangent matrix for the drill RC has one spurious zero eigenvalue; the associated eigenvector Θ_2 is shown in Fig. 12.9b. The simplest way of treating this deficiency is

to apply eq. (12.143), which provides the stabilization matrix $\mathbf{K}^{\text{stab}}_{\omega\omega}$ of eq. (12.144), so we have

$$\mathbf{K}_{\omega\omega} + \mathbf{K}^{\text{stab}}_{\omega\omega}, \tag{12.25}$$

where $\mathbf{K}_{\omega\omega}$ is the rank-deficient matrix obtained by differentiating twice the drill RC term modified as given either in eq. (12.23) or in eq. (12.24).

Expansion of $\mathbf{Q}^T\mathbf{F}$ product. The linear expansion of $c(\xi,\eta)$ of eq. (12.23) can be obtained in the following way. First, we expand $\mathbf{Q}$ and $\mathbf{F}$ at the element's center,

$$\mathbf{Q}(\xi,\eta) \doteq \mathbf{Q}_c + \xi\,\mathbf{Q}_{,\xi c} + \eta\,\mathbf{Q}_{,\eta c}, \qquad \mathbf{F}(\xi,\eta) \doteq \mathbf{F}_c + \xi\,\mathbf{F}_{,\xi c} + \eta\,\mathbf{F}_{,\eta c}, \tag{12.26}$$

where $(\,)_{,\xi c} \doteq (\,)_{,\xi}\big|_c$ and $(\,)_{,\eta c} \doteq (\,)_{,\eta}\big|_c$. Then, we calculate the $\mathbf{Q}^T\mathbf{F}$ product, in which we retain only the constant and linear terms,

$$\mathbf{Q}^T(\xi,\eta)\,\mathbf{F}(\xi,\eta) \approx \mathbf{Q}_c^T\mathbf{F}_c + \xi\left(\mathbf{Q}_c^T\mathbf{F}_{,\xi c} + \mathbf{Q}_{,\xi c}^T\mathbf{F}_c\right) + \eta\left(\mathbf{Q}_c^T\mathbf{F}_{,\eta c} + \mathbf{Q}_{,\eta c}^T\mathbf{F}_c\right), \tag{12.27}$$

while bilinear and quadratic terms are omitted. Finally,

$$c(\xi,\eta) \doteq \left[\text{skew}(\mathbf{Q}^T\mathbf{F})\right]_{12}, \tag{12.28}$$

i.e. we calculate the skew-symmetric part of the matrix and, provided that the matrix is given in the local Cartesian basis, we use the 12 component.

Enhancement resulting from bi-quadratic approximations of displacements. Another way of addressing the problem with the bilinear term in eq. (12.20) is to enhance displacements in such a way that ω_3 is linked with enhancing parameters.

The enhancing modes can be selected upon analysis of bi-quadratic approximations of displacements of the nine-node Lagrangian element shown in Fig. 12.3. For the bi-quadratic approximations, the vector of shape functions is defined as

$$\mathbf{N} \doteq \{P_1Q_1, P_3Q_1, P_3Q_3, P_1Q_3, P_2Q_1, P_3Q_2, P_2Q_3, P_1Q_2, P_2Q_2\}, \tag{12.29}$$

where each component is a product of P_i and Q_j, $i,j \in \{1,2,3\}$, defined as

$$P_1 \doteq \tfrac{1}{2}(\xi^2 - \xi), \qquad P_2 \doteq 1 - \xi^2, \qquad P_3 \doteq \tfrac{1}{2}(\xi^2 + \xi),$$

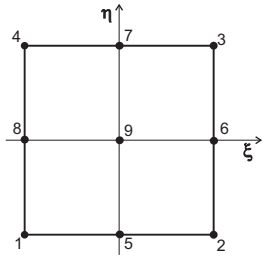

Fig. 12.3 Numeration of nodes on a nine-node Lagrangian element.

$$Q_1 \doteq \tfrac{1}{2}(\eta^2 - \eta), \qquad Q_2 \doteq 1 - \eta^2, \qquad Q_3 \doteq \tfrac{1}{2}(\eta^2 + \eta).$$

Using $\mathbf{N}$ for each displacement component separately, we have

$$u = u_0 + u_1\,\xi + u_2\,\eta + u_3\,\xi\eta + u_4\,\xi^2 + u_5\,\eta^2 + u_6\,\xi\eta^2 + u_7\,\xi^2\eta + u_8\,\xi^2\eta^2,$$
$$v = v_0 + v_1\,\xi + v_2\,\eta + v_3\,\xi\eta + v_4\,\xi^2 + v_5\,\eta^2 + v_6\,\xi\eta^2 + v_7\,\xi^2\eta + v_8\,\xi^2\eta^2,$$

where $u_i,\, v_i \quad (i = 0, \ldots, 8)$ are functions of nodal values of respective displacement components.

For simplicity, we consider a 2×2 square element with the center located at the origin of the Cartesian coordinate system. Then the bilinear term of the drill RC of eq. (12.19) yields the equation

$$u_7 - v_6 + \omega_3 = 0. \tag{12.30}$$

Using this equation, the $\xi\eta$ mode of drilling rotation is linked with the $\xi^2\eta$ and $\xi\eta^2$ modes of displacements. These modes are not available in a four-node bilinear element, but can be included as the EADG enhancement.

Let us assume the incompatible displacements in the form

$$u^{\mathrm{inc}} = q_5\,\xi^2\eta, \qquad v^{\mathrm{inc}} = q_6\,\xi\eta^2, \tag{12.31}$$

where q_5, q_6 are unknown multipliers. Then

$$\mathbf{G}_2^{\xi} \doteq \begin{bmatrix} \frac{\partial u^{\mathrm{inc}}}{\partial \xi} & \frac{\partial u^{\mathrm{inc}}}{\partial \eta} \\ \frac{\partial v^{\mathrm{inc}}}{\partial \xi} & \frac{\partial v^{\mathrm{inc}}}{\partial \eta} \end{bmatrix} = \begin{bmatrix} 2q_5\,\xi\eta & q_5\,\xi^2 \\ q_6\,\eta^2 & 2q_6\,\xi\eta \end{bmatrix},$$

where we have the $\xi\eta$ term on the diagonal. This matrix should be added to $\mathbf{G}^{\xi}$ in eq. (11.71) for the EADG enhancement.

We implemented the element based on the potential energy, the EADG4 enhancement, and the above-defined enhancement, but the displacements and rotations in Cook's membrane example of Sect. 15.2.7 were excessive.

12.3 Implementation of drill RC in finite elements

Overview. The drilling rotations are included in shell elements with the purpose of having three rotational degrees of freedom at each node and to facilitate linking the elements of various spatial orientation. Several methods can be applied to develop the finite element with the drilling rotation.

1. Basic method. The basic method amounts to appending the drill RCs evaluated at some points to the elemental set of equations. The method is simple but the tangent matrix is non-symmetric.

2. Methods of constrained optimization. The methods of constrained optimization, see [136, 72, 29], yield a symmetric tangent matrix, but are more complicated than the basic method. The optimization problem is defined as follows:

$$\min_{(\mathbf{u},\mathbf{Q})} F(\mathbf{u}) \qquad \text{subject to} \quad \mathbf{c}(\mathbf{u},\mathbf{Q}) = \mathbf{0}, \tag{12.32}$$

where F is the governing functional and $\mathbf{c}(\mathbf{u},\mathbf{Q}) = \mathbf{0}$ is the set of constraints related to the drill RC equation. Note that

1. various functional can be used as F, including the potential energy F_{PE}, the HR functional F_{HR}, and the HW functional F_{HW} of Sect. 11.1. However, for each functional, an optimal finite element must be developed separately.
2. Several forms of the constraint can be formulated for the drill RC equation, including strong and weak (integral) forms,
3. Several methods can be used to solve this problem of constrained optimization; in our elements we use either the penalty method or the Perturbed Lagrange method.

Below, for simplicity, we consider the potential energy $F_{\mathrm{PE}}(\mathbf{u}) \doteq \int_B \mathcal{W}(\mathbf{u})\, \mathrm{d}V - F_{\mathrm{ext}}$. The extended functional which is constructed for the above-constrained optimization problem includes the part related to the drill RC equation, which can be written in two forms:

A. Strong form. Let us write the constraint related to drill RC equation as $c = 0$. We can evaluate $c(\xi,\eta)$ at four selected points within an element and form a vector, $\mathbf{c} \doteq \{c_1, c_2, c_3, c_4\}$, which is used by the strong forms discussed below.

The penalty method is based on the following extended functional,

$$F'_{\mathrm{PE}}(\mathbf{u},\mathbf{Q}) \doteq F_{\mathrm{PE}}(\mathbf{u}) + \frac{\gamma}{2}\mathbf{c}\cdot\mathbf{c}, \tag{12.33}$$

where $\gamma > 0$ is the penalty parameter. Minimization is performed w.r.t. the nodal values of $(\mathbf{u},\mathbf{Q})$. The definition of γ depends on material coefficients and the element's volume, to preserve the same degree of penalization for various volumes.

The perturbed Lagrange method is based on the following extended functional

$$F'_{\mathrm{PE}}(\mathbf{u},\mathbf{Q},\boldsymbol{\lambda}) \doteq F_{\mathrm{PE}}(\mathbf{u}) + \boldsymbol{\lambda}\cdot\mathbf{c} + \frac{1}{2\gamma}\boldsymbol{\lambda}\cdot\boldsymbol{\lambda}, \tag{12.34}$$

where $\boldsymbol{\lambda} \doteq \{\lambda_1,\lambda_2,\lambda_3,\lambda_4\}$ is a vector of Lagrange multipliers, with each multiplier for $c = 0$ written at a point within an element. Minimization is performed w.r.t. nodal values of $(\mathbf{u},\mathbf{Q})$ and the elemental vector $\boldsymbol{\lambda}$.

B. Weak (integral) form. The part related to the drill RC can also be formulated in an integral form, resembling the form of the strain energy, which is an integral over the element volume, $\int_B \mathcal{W}(\mathbf{u})\,\mathrm{d}V$. Let the drill RC have the form $c(\xi,\eta) = 0$.

The penalty method is based on the following extended functional:

$$F'_{\mathrm{PE}}(\mathbf{u},\mathbf{Q}) \doteq F_{\mathrm{PE}}(\mathbf{u}) + \int_B \frac{\gamma}{2}\,c^2\,\mathrm{d}V, \tag{12.35}$$

where $\gamma > 0$ is the penalty parameter. Minimization is performed w.r.t. the nodal values of $(\mathbf{u},\mathbf{Q})$. The volume of the element is automatically accounted for by the integral formulation, so it suffices to relate γ to material coefficients.

The perturbed Lagrange method is based on the following extended functional:

$$F'_{\mathrm{PE}}(\mathbf{u},\mathbf{Q},\boldsymbol{\lambda}) \doteq F_{\mathrm{PE}}(\mathbf{u}) + \int_B \left(\lambda\,c + \frac{1}{2\gamma}\lambda^2\right)\,\mathrm{d}V, \tag{12.36}$$

where λ is the Lagrange multiplier which must be approximated (assumed) over the element. Minimization is performed w.r.t. the nodal values of $(\mathbf{u},\mathbf{Q})$ and the elemental parameters of λ.

The weak forms correspond to the variational formulations of Sect. 4, and were used in implementation of our elements.

12.3.1 Selected methods to include the drill RC

Below we discuss selected methods used to include the drilling rotations in FE equations, such as the basic method, the penalty method, and the Perturbed Lagrange method.

1. Basic method

The basic method consists of two steps:

1. The drill RC equation is expanded as specified by eq. (12.23), and evaluated at four selected points within an element, which yields the equation $\mathbf{r}_\omega = \mathbf{0}$, where $\mathbf{r}_\omega \doteq \{r_{\omega 1}, r_{\omega 2}, r_{\omega 3}, r_{\omega 4}\}$. The linearized (Newton) form of this equation is

$$\mathbf{K}_{\omega u} \Delta \mathbf{u}_I + \mathbf{K}_{\omega\omega} \Delta \boldsymbol{\omega}_I = -\mathbf{r}_\omega, \tag{12.37}$$

   where $\mathbf{u}_I \doteq \{\mathbf{u}_1, \mathbf{u}_2, \mathbf{u}_3, \mathbf{u}_4\}$ and $\boldsymbol{\omega}_I \doteq \{\omega_1, \omega_2, \omega_3, \omega_4\}$ are vectors of displacements and drilling rotations at nodes, and the matrices are

$$\mathbf{K}_{\omega\omega} \doteq \frac{\partial \mathbf{r}_\omega}{\partial \boldsymbol{\omega}_I}, \qquad \mathbf{K}_{\omega u} \doteq \frac{\partial \mathbf{r}_\omega}{\partial \mathbf{u}_I}.$$

   The drill RC equation can be used in one of the forms specified in eqs. (12.7), (12.9), and (12.10); in computations, we used the last one.
2. Equation (12.37) is appended to the set of FE equations for a purely displacement problem, $\mathbf{K}\ \Delta \mathbf{u}_I = -\mathbf{r}$, where

$$\mathbf{r} \doteq \frac{\partial F_{\mathrm{PE}}(\mathbf{u}_I)}{\partial \mathbf{u}_I}, \qquad \mathbf{K} \doteq \frac{\partial \mathbf{r}}{\partial \mathbf{u}_I}.$$

   This yields

$$\begin{bmatrix} \mathbf{K} & \mathbf{0} \\ \mathbf{K}_{\omega u} & \mathbf{K}_{\omega\omega} \end{bmatrix} \begin{bmatrix} \Delta \mathbf{u}_I \\ \Delta \boldsymbol{\omega}_I \end{bmatrix} = - \begin{bmatrix} \mathbf{r} \\ \mathbf{r}_\omega \end{bmatrix}. \tag{12.38}$$

   This is a set of equations for an element. By aggregation of such sets for all elements, we obtain the global tangent matrix, which must be non-singular to provide a unique solution. The increments of displacements and drilling rotations at nodes are computed together.

Note that the matrix in eq. (12.38) is non-symmetric, which is a disadvantage, as symmetric solvers are faster. If a non-symmetric solver is used for other reasons, then this formulation also is suitable.

Consider stability of the basic formulation. We assume that the boundary conditions are accounted for in the set (12.38). From the first equation

of (12.38), we calculate $\Delta\mathbf{u}_I = -\mathbf{K}^{-1}\mathbf{r}$ and using it in the second equation, we obtain

$$\Delta\boldsymbol{\omega}_I = -\mathbf{K}_{\omega\omega}^{-1}(\mathbf{r}_\omega - \mathbf{K}_{\omega u}\mathbf{K}^{-1}\mathbf{r}). \tag{12.39}$$

Let us write this equation at $\mathbf{u}_I = \mathbf{0}$ and $\boldsymbol{\omega}_I = \mathbf{0}$. Then, the residuals $\mathbf{r}_u = \mathbf{0}$, $\mathbf{r}_\omega = \mathbf{0}$, and $\mathbf{r} = -\mathbf{p}$, where $\mathbf{p}$ is a vector of external loads for translational dofs, and we obtain

$$\Delta\boldsymbol{\omega}_I = -(\mathbf{K}_{\omega\omega}^{-1}\mathbf{K}_{\omega u}\mathbf{K}^{-1})\ \mathbf{p}. \tag{12.40}$$

Hence, to uniquely compute the solution, $\mathbf{K}$ and $\mathbf{K}_{\omega\omega}$ must be invertible. Note that

1. elimination of ω_3 from eq. (12.20) means that $\mathbf{K}_{\omega\omega}$ becomes singular and must be stabilized, as given by eq. (12.25).
2. The drill RC cannot be evaluated at mid-side edge points, as then $\mathbf{K}_{\omega\omega}$ has complex eigenvalues, see the example below. The Gauss points or the corner nodes are good locations.

Example. Consider the single trapezoidal element of Fig. 15.1b, obtained for $d = 0.5$, and $E = 10^6$, $\nu = 0.3$, $h = 0.1$. The standard element Q4 and the basic method for the drill RC were used.

The eigenvalues of $\mathbf{K}_{\omega\omega}$ obtained for various locations of the evaluation points are shown in Table 12.1 and we see that they differ and do not depend on the element's shape, a specific property of $\mathbf{K}_{\omega\omega}$! For the mid-side nodes, we obtain two complex eigenvalues!

Table 12.1 Basic method. Eigenvalues of $\mathbf{K}_{\omega\omega}$.

Drill RC evaluated at	Eigenvalues (truncated)			
trapezoidal element				
Gauss points	2	1.15	1.15	0.66
corner nodes	2	2	2	2
mid-side nodes	2	1+i	1-i	0
square element				
Gauss points	2	1.15	1.15	0.66
corner nodes	2	2	2	2
mid-side nodes	2	1+i	1-i	0

Besides, we consider stretching the element in a vertical direction. Two parallel and equal forces are applied at the top nodes, while the boundary conditions eliminating rigid body modes are applied to displacements

at the bottom nodes. The calculated drilling rotations are shown in Table 12.2, and we see that they are different for various location of the evaluation points. These differences vanish for a square element, $d = 0$.

Table 12.2 Basic method. Drilling rotations for stretched element.

Drill RC evaluated at	Drilling rotation at nodes			
trapezoidal element				
Gauss points	0.310	0.210	0.581	0.771
corner nodes	0.280	0.195	0.574	0.756
square element				
Gauss points	0	0	0	0
corner nodes	0	0	0	0

2. Penalty method

The penalty method is a classical method of solving problems of constrained optimization, [72, 29]. Generally, it is defined as a sequence of unconstrained optimization problems, which are solved for selected increasing values of the penalty parameter, [72] eq. (12.1.4). However, for efficiency reasons, the shortcut method is used in practice and not a sequence of problems, but a single unconstrained optimization problem is solved for a largish value of the penalty parameter. Hence, some errors are inevitable and we try to minimize them by selecting a suitable value of the penalty parameter; this issue is discussed in Sect. 12.3.2.

The penalty method can be used with the drill RC term in one of the previously mentioned two forms:

1. the strong form of eq. (12.33), for which we can consider several locations to evaluate the drill RC, similarly as for the basic method. For the penalty method, however, the matrix $\mathbf{K}_{\omega\omega}$ has no complex eigenvalues, for any of the considered locations.
2. the weak form of eq. (12.35), for which the drill RC is evaluated at Gauss points. Because of the integral form, the weak form automatically accounts for the element volume, so it suffices to relate the penalty coefficient γ to material coefficients.

Note that if the strong form is evaluated at Gauss points, then the only difference between these two forms are the determinants of the Jacobian used in the weak form.

The scalar drill RC equation can be used in one of the three forms specified in eqs. (12.7), (12.9), and (12.10); in computations we used the last one.

The weak form is discussed in detail below.

Relation of weak form of eq. (12.35) to variational formulation of Sect. 4. Recall the formulation based on the second Piola-Kirchhoff stress and the 3-F functional of eq. (4.65). This functional was regularized in $\mathbf{T}_a$, which is the Lagrange multiplier for the RC equation (3.8). Then, using the Euler–Lagrange equation for $\delta\mathbf{T}_a$, i.e. $\mathbf{T}_a = \gamma\,\mathrm{skew}(\mathbf{Q}^T\mathbf{F})$, we obtained the 2-F functional of eq. (4.73), which we repeat it here as

$$\tilde{F}_2^{\mathrm{2PK}}(\boldsymbol{\chi},\mathbf{Q}) \doteq \int_B \left[\mathcal{W}(\mathbf{F}^T\mathbf{F}) + F_{\mathrm{RC}}^{\mathrm{P}}(\boldsymbol{\chi},\mathbf{Q})\right]\,\mathrm{d}V + F_{\mathrm{ext}}, \tag{12.41}$$

where the penalty term for the RC equation is

$$F_{\mathrm{RC}}^{\mathrm{P}}(\boldsymbol{\chi},\mathbf{Q}) \doteq \frac{\gamma}{2}\mathrm{skew}(\mathbf{Q}^T\mathbf{F})\cdot\mathrm{skew}(\mathbf{Q}^T\mathbf{F}). \tag{12.42}$$

If we restrict our considerations to a 2D problem, then the RC equation is reduced to the drill RC equation. For $\mathbf{Q}$ and $\mathbf{F}$ of eq. (12.3), we obtain $\mathrm{skew}(\mathbf{Q}^T\mathbf{F})$ of eq. (12.4), for which

$$F_{\mathrm{RC}}^{\mathrm{P}}(\boldsymbol{\chi},\mathbf{Q}) = \frac{\gamma}{2}2\,r_\omega^2. \tag{12.43}$$

Comparing this expression for F_{RC} with the drill term in the weak form, eq. (12.35), which is $(\gamma/2)\,r_\omega^2$, we see that the difference between them is the multiplier 2, which is a result of two identical (except for the sign) terms of the skew-symmetric matrix. Hence, functional (12.41) fully corresponds to the weak form of eq. (12.35).

Linearized equations. The standard procedure of consistent linearization of the functionals for the penalty method yields the following linearized (Newton) equations:

$$\left(\begin{bmatrix}\mathbf{K} & \mathbf{0}\\ \mathbf{0} & \mathbf{0}\end{bmatrix} + \gamma\begin{bmatrix}\mathbf{K}_{uu} & \mathbf{K}_{u\omega}\\ \mathbf{K}_{\omega u} & \mathbf{K}_{\omega\omega}\end{bmatrix}\right)\begin{Bmatrix}\Delta\mathbf{u}_I\\ \Delta\boldsymbol{\omega}_I\end{Bmatrix} = -\begin{Bmatrix}\mathbf{r}+\gamma\mathbf{r}_u\\ \gamma\mathbf{r}_\omega\end{Bmatrix}, \tag{12.44}$$

where

$$\mathbf{r}_u \doteq \frac{\partial F_{\mathrm{RC}}}{\partial\mathbf{u}_I}, \qquad \mathbf{K}_{uu} \doteq \frac{\partial\mathbf{r}_u}{\partial\mathbf{u}_I}, \qquad \mathbf{K}_{u\omega} \doteq \frac{\partial\mathbf{r}_u}{\partial\boldsymbol{\omega}_I},$$

$$\mathbf{r}_\omega \doteq \frac{\partial F_{\mathrm{RC}}}{\partial \boldsymbol{\omega}_I}, \qquad \mathbf{K}_{\omega\omega} \doteq \frac{\partial \mathbf{r}_\omega}{\partial \boldsymbol{\omega}_I}, \qquad \mathbf{K}_{\omega u} \doteq \frac{\partial \mathbf{r}_\omega}{\partial \mathbf{u}_I}.$$

The tangent matrix is symmetric, unlike the one for the basic method of eq. (12.38). The above-defined vectors and matrices do not depend on the penalty parameter γ; its value is selected as described in the next section.

Elimination of ω_3 from eq. (12.20) means that $\mathbf{K}_{\omega\omega}$ becomes singular and must be stabilized, as given by eq. (12.25), to ensure its invertibility.

Let us write eq. (12.44) at $\mathbf{u}_I = \mathbf{0}$ and $\boldsymbol{\omega}_I = \mathbf{0}$. Then the residuals $\mathbf{r}_u = \mathbf{0}$, $\mathbf{r}_\omega = \mathbf{0}$, and $\mathbf{r} = -\mathbf{p}$, where $\mathbf{p}$ is a vector of external loads for translational dofs, and we obtain

$$\left(\begin{bmatrix} \mathbf{K} & \mathbf{0} \\ \mathbf{0} & \mathbf{0} \end{bmatrix} + \gamma \begin{bmatrix} \mathbf{K}_{uu} & \mathbf{K}_{u\omega} \\ \mathbf{K}_{\omega u} & \mathbf{K}_{\omega\omega} \end{bmatrix} \right) \begin{bmatrix} \Delta\mathbf{u}_I \\ \Delta\boldsymbol{\omega}_I \end{bmatrix} = \begin{bmatrix} \mathbf{p} \\ \mathbf{0} \end{bmatrix}. \tag{12.45}$$

We assume that the boundary conditions are accounted for in this set and consider the stability requirements for the following two particular solution processes.

A. From the second equation of the set (12.45), we calculate

$$\Delta\boldsymbol{\omega}_I = -\mathbf{K}_{\omega\omega}^{-1}\mathbf{K}_{\omega u}\Delta\mathbf{u}_I \tag{12.46}$$

and use it in the first equation, which yields

$$(\mathbf{K} + \gamma\mathbf{K}_1)\ \Delta\mathbf{u}_I = \mathbf{p}, \tag{12.47}$$

where $\mathbf{K}_1 \doteq \mathbf{K}_{uu} - \mathbf{K}_{u\omega}\mathbf{K}_{\omega\omega}^{-1}\mathbf{K}_{\omega u}$. Hence, the stability requires invertibility of $\mathbf{K}_{\omega\omega}$ and $\mathbf{K} + \gamma\mathbf{K}_1$.

B. Much more complicated stability conditions are obtained if we change the order in which $\Delta\boldsymbol{\omega}_I$ and $\Delta\mathbf{u}_I$ are calculated. Then, from the first equation of the set (12.44), we calculate

$$\Delta\mathbf{u}_I = \mathbf{K}_*^{-1}(\mathbf{p} - \gamma\mathbf{K}_{u\omega}\Delta\boldsymbol{\omega}_I), \tag{12.48}$$

where $\mathbf{K}_* \doteq \mathbf{K} + \gamma\mathbf{K}_{uu}$, and using it in the second equation, we obtain

$$\Delta\boldsymbol{\omega}_I = -\mathbf{K}_{**}^{-1}\mathbf{K}_{\omega u}\mathbf{K}_*^{-1}\mathbf{p}, \tag{12.49}$$

where $\mathbf{K}_{**} \doteq \mathbf{K}_{\omega\omega} - \gamma \mathbf{K}_{\omega u} \mathbf{K}_{*}^{-1} \mathbf{K}_{u\omega}$. To obtain a stable formulation, we need the invertibility of $\mathbf{K}_{*}$ and $\mathbf{K}_{**}$, so we have to satisfy two conditions,

$$\det \mathbf{K}_{*}(\gamma) \neq 0, \qquad \det \mathbf{K}_{**}(\gamma) \neq 0. \tag{12.50}$$

They are too complicated to determine analytically which values of γ are not admissible.

Neither one of the solution processes **A** and **B** is applicable to a general problem, involving many elements and boundary conditions for displacements and drilling rotations. Then we have to consider the whole set (12.44) and invertibility of the global tangent matrix is required.

Remark on the Augmented Lagrange method. We have also implemented the Augmented Lagrange (AuL) method as an extension of the penalty method, requiring only minor modifications of the code. The update formula for the Lagrange multiplier of [179] was applied and several approximations of the Lagrange multiplier were tested. In linear tests, the AuL method performs identically to the penalty method, but in nonlinear tests, e.g. in the pinched hemisphere with a hole of Sect. 15.3.8, the performance was worse than that of the penalty method.

Example. Single element. Consider a single element of Fig. 15.1b, with $E = 10^6$, $\nu = 0.3$, $h = 0.1$. The non-enhanced element Q4 and the penalty method for the drill RC were used.

The matrix $\mathbf{K}_1$ of eq. (12.47) was calculated for two element shapes, trapezoid ($d = 0.5$) and square ($d = 0$), and the boundary conditions were either applied or not applied. In all these cases, $\mathbf{K}_1 = \mathbf{0}$. Hence, the correct solution,

$$\Delta \mathbf{u}_I = \mathbf{K}^{-1} \mathbf{p}, \qquad \Delta \boldsymbol{\omega}_I = -\mathbf{K}_{\omega\omega}^{-1} \mathbf{K}_{\omega u} \Delta \mathbf{u}_I, \tag{12.51}$$

is obtained for any value of $\gamma > 0$; this is a feature of the so-called *exact* penalty method. A similar result is obtained for the formulation with the drilling rotation being a local variable, discontinuous across the element's boundaries.

The determinants of matrices $\mathbf{K}_{*}$ and $\mathbf{K}_{**}$ for selected values of γ are given in Table 12.3. We see that they are all non-zero, as required.

Table 12.3 Determinants of $\mathbf{K}_*$ and $\mathbf{K}_{**}$ for the penalty method.

Multiplier γ	$\det \mathbf{K}_*$	$\det \mathbf{K}_{**}$
trapezoidal element		
1	10^{22}	10^{-6}
G/1000	10^{23}	10^{4}
G	10^{38}	10^{1}
1000 G	10^{56}	10^{28}

3. Perturbed Lagrange method

The Perturbed Lagrange method belongs to the class of the Lagrange–Newton methods of the constrained optimization, see [136, 72, 29], to which the popular SQP (Sequential Quadratic Programming) method also belongs. For this class, the Newton method is used to find the stationary point of the Lagrange function w.r.t. the basic variables and the Lagrange multipliers.

In the Perturbed Lagrange method, a small perturbation term is defined in terms of the Lagrange multipliers and added to the standard Lagrange function. In computational contact mechanics, which involves inequality constraints, this method was used, e.g., in [157, 222]. For contact problems, the role of the perturbation component is to fill in the zero sub-matrix when the gap is open, see [261], eqs. (5.58) and (9.75).

The Perturbed Lagrange method can also be applied to the drill RC problem and it enables us to treat the Lagrange multipliers as local variables and to eliminate them on the element's level. Besides, we can use a simple symmetric solver on the element's level because there is no zero diagonal blocks.

The Perturbed Lagrange method can be used with the drill RC term in two forms: either the strong form of eq. (12.34) or the weak form of eq. (12.36). For both, we can use the scalar drill RC equation in one of the three forms specified in eqs. (12.7), (12.9), and (12.10); in computations we use the last one.

Relation of weak form of eq. (12.36) to variational formulation of Sect. 4. Recall the formulation based on the second Piola-Kirchhoff stress, and the three-field functional of eq. (4.65). This functional was regularized in $\mathbf{T}_a$, where $\mathbf{T}_a$ is the Lagrange multiplier for the RC equation (3.8), which yielded the 3-F functional of eq. (4.71), which we repeat here in the following form:

$$\tilde{F}_3^{\mathrm{2PK}}(\boldsymbol{\chi}, \mathbf{Q}, \mathbf{T}_a) = \int_B \left[\mathcal{W}(\mathbf{F}^T\mathbf{F}) + F_{\mathrm{RC}}(\boldsymbol{\chi}, \mathbf{Q}, \mathbf{T}_a)\right] \mathrm{d}V - F_{\mathrm{ext}}, \quad (12.52)$$

where

$$F_{\mathrm{RC}}^{\mathrm{PL}}(\boldsymbol{\chi}, \mathbf{Q}, \mathbf{T}_a) \doteq \mathbf{T}_a \cdot \mathrm{skew}(\mathbf{Q}^T\mathbf{F}) - \frac{1}{2\gamma}\mathbf{T}_a \cdot \mathbf{T}_a \quad (12.53)$$

and $\gamma \in (0, \infty)$ is the regularization parameter. If we restrict our considerations to a 2D problem, then the RC equation is reduced to the drill RC equation. For $\mathbf{Q}$ and $\mathbf{F}$ of eq. (12.3), from $\mathrm{skew}(\mathbf{Q}^T\mathbf{F})$ we obtain r_ω, as in eq. (12.4). Besides, the Lagrange multiplier is assumed to be in the following form:

$$\mathbf{T}_a \doteq \begin{bmatrix} 0 & -T \\ T & 0 \end{bmatrix}. \quad (12.54)$$

see eq. (12.56) for more details. For these representations, we obtain $\mathbf{T}_a \cdot \mathrm{skew}(\mathbf{Q}^T\mathbf{F}) = 2Tr_\omega$ and $\mathbf{T}_a \cdot \mathbf{T}_a = 2T^2$, and eq. (12.53) becomes

$$F_{\mathrm{RC}}^{\mathrm{PL}}(\boldsymbol{\chi}, \mathbf{Q}, \mathbf{T}_a) = 2\left(T\, r_\omega - \frac{1}{2\gamma}T^2\right). \quad (12.55)$$

Comparing this expression with the drill term in the weak form eq. (12.36), which is $\lambda\, c + (1/2\gamma)\lambda^2$, we see that the difference between them is the multiplier 2, which is a result of two identical (except for the sign) terms of the skew-symmetric matrices. Hence, functional (12.41) fully corresponds to the weak form of eq. (12.36).

Approximation of $F_{\mathrm{RC}}^{\mathrm{PL}}$. Various approximations of the functional F_{RC} of eq. (12.55) can be considered for a four-node element, and we selected the following ones:

1. the Lagrange multiplier is assumed as a contravariant matrix in the basis $\{\mathbf{g}_k^c\}$ and is transformed to the local orthonormal basis $\{\mathbf{t}_k^c\}$ as follows:

$$\mathbf{T}_a = \mathbf{J}_{Lc}\begin{bmatrix} 0 & T_a(\xi,\eta) \\ -T_a(\xi,\eta) & 0 \end{bmatrix}\mathbf{J}_{Lc}^T = \begin{bmatrix} 0 & T \\ -T & 0 \end{bmatrix}, \quad (12.56)$$

where $T_a(\xi,\eta)$ is the assumed representation of the Lagrange multiplier, and $T \doteq (\det \mathbf{J}_{Lc})\, T_a(\xi,\eta)$, as the $\mathbf{J}_{Lc}(\cdot)\,\mathbf{J}_{Lc}^T$ operation on a skew-symmetric matrix yields a skew-symmetric matrix. This T was used in eq. (12.54). The Jacobian is local, as both bases are located at the element's center.

2. A linear approximation of the assumed representation of the Lagrange multiplier,
$$T_a(\xi,\eta) \doteq q_0 + \xi\, q_1 + \eta\, q_2, \tag{12.57}$$
where q_0, q_1, q_2 are local multipliers eliminated on the element's level.
3. A linear expansion of the drill rotation constraint, $c = 0$, at the element center of eq. (12.28), for which the bilinear term of the drill RC of eq. (12.20) is eliminated.

Linearized equations. The standard procedure of consistent linearization of the functionals for the Perturbed Lagrange method yields the following linearized (Newton) equations:

$$\begin{bmatrix} \mathbf{K} & \mathbf{K}_{u\omega} & \mathbf{K}_{uT} \\ \mathbf{K}_{u\omega}^T & \mathbf{K}_{\omega\omega} & \mathbf{K}_{\omega T} \\ \mathbf{K}_{uT}^T & \mathbf{K}_{\omega T}^T & -\frac{1}{\gamma}\mathbf{K}_{TT} \end{bmatrix} \begin{bmatrix} \Delta\mathbf{u}_I \\ \Delta\boldsymbol{\omega}_I \\ \Delta\mathbf{T}_a \end{bmatrix} = - \begin{bmatrix} \mathbf{r} + \mathbf{r}_u \\ \mathbf{r}_\omega \\ \mathbf{r}_T \end{bmatrix}, \tag{12.58}$$

where the vectors and matrices obtained from $F_{\mathrm{RC}}^{\mathrm{PL}}$ of eq. (12.55) are as follows:

$$\mathbf{r}_u \doteq \frac{\partial F_{\mathrm{RC}}}{\partial \mathbf{u}_I}, \quad \mathbf{K}_{uu} \doteq \frac{\partial \mathbf{r}_u}{\partial \mathbf{u}_I}, \quad \mathbf{K}_{u\omega} \doteq \frac{\partial \mathbf{r}_u}{\partial \boldsymbol{\omega}_I}, \quad \mathbf{K}_{uT} \doteq \frac{\partial \mathbf{r}_u}{\partial \mathbf{T}_a},$$
$$\mathbf{r}_\omega \doteq \frac{\partial F_{\mathrm{RC}}}{\partial \boldsymbol{\omega}_I}, \quad \mathbf{K}_{\omega\omega} \doteq \frac{\partial \mathbf{r}_\omega}{\partial \boldsymbol{\omega}_I}, \quad \mathbf{K}_{\omega u} \doteq \frac{\partial \mathbf{r}_\omega}{\partial \mathbf{u}_I}, \quad \mathbf{K}_{\omega T} \doteq \frac{\partial \mathbf{r}_\omega}{\partial \mathbf{T}_a},$$
$$\mathbf{r}_T \doteq \frac{\partial F_{\mathrm{RC}}}{\partial \mathbf{T}_a}, \quad \mathbf{K}_{T\omega} \doteq \frac{\partial \mathbf{r}_T}{\partial \boldsymbol{\omega}_I}, \quad \mathbf{K}_{Tu} \doteq \frac{\partial \mathbf{r}_T}{\partial \mathbf{u}_I}, \quad \mathbf{K}_{TT} \doteq \frac{\partial \mathbf{r}_T}{\partial \mathbf{T}_a}.$$

Note that $\mathbf{K}_{uu} = \mathbf{0}$. The total matrix is symmetric because $\mathbf{K} = \mathbf{K}^T$, $\mathbf{K}_{\omega\omega} = \mathbf{K}_{\omega\omega}^T$, $\mathbf{K}_{TT} = \mathbf{K}_{TT}^T$, as well as $\mathbf{K}_{\omega u} = \mathbf{K}_{u\omega}^T$, $\mathbf{K}_{Tu} = \mathbf{K}_{uT}^T$, and $\mathbf{K}_{T\omega} = \mathbf{K}_{\omega T}^T$.

Let us write the set of eq. (12.58) for $\mathbf{u}_I = \mathbf{0}$ and $\boldsymbol{\omega}_I = \mathbf{0}$. Then the residuals $\mathbf{r}_u = \mathbf{0}$, $\mathbf{r}_\omega = \mathbf{0}$, $\mathbf{r}_T = \mathbf{0}$, and $\mathbf{r} = -\mathbf{p}$, where $\mathbf{p}$ is a vector of external loads for translational dofs. For the applied approximations of displacements and drilling rotations, we obtain

$$\begin{bmatrix} \mathbf{K} & \mathbf{0} & \mathbf{K}_{uT} \\ \mathbf{0} & \mathbf{0} & \mathbf{K}_{\omega T} \\ \mathbf{K}_{uT}^T & \mathbf{K}_{\omega T}^T & -\frac{1}{\gamma}\mathbf{K}_{TT} \end{bmatrix} \begin{bmatrix} \Delta\mathbf{u}_I \\ \Delta\boldsymbol{\omega}_I \\ \Delta\mathbf{T}_a \end{bmatrix} = \begin{bmatrix} \mathbf{p} \\ \mathbf{0} \\ \mathbf{0} \end{bmatrix}. \tag{12.59}$$

In the *standard* Lagrange multiplier method, the perturbation term is neglected in eq. (12.55) and, then in the above matrix, the perturbation matrix $\mathbf{K}_{TT}$ is a zero matrix.

Because, the bilinear terms are omitted in the representations of eqs. (12.57) and (12.23), the element has one spurious zero eigenvalue and can be stabilized, as given by eq. (12.25). Then, eq. (12.59) becomes

$$\begin{bmatrix} \mathbf{K} & \mathbf{0} & \mathbf{K}_{uT} \\ \mathbf{0} & \mathbf{K}_{\omega\omega}^{\text{stab}} & \mathbf{K}_{\omega T} \\ \mathbf{K}_{uT}^T & \mathbf{K}_{\omega T}^T & -\frac{1}{\gamma}\mathbf{K}_{TT} \end{bmatrix} \begin{bmatrix} \Delta\mathbf{u}_I \\ \Delta\boldsymbol{\omega}_I \\ \Delta\mathbf{T}_a \end{bmatrix} = \begin{bmatrix} \mathbf{p} \\ \mathbf{0} \\ \mathbf{0} \end{bmatrix}, \tag{12.60}$$

where the matrix $\mathbf{K}_{\omega\omega}^{\text{stab}}$ is provided by stabilization, and the number of zero eigenvalues is three, as required.

Stability of solution for local Lagrange multiplier. Assume that the parameters q_i of the Lagrange multiplier $\mathbf{T}_a$ are *local* variables, which are discontinues across the element boundaries and are eliminated on the element level. Then, first we calculate $\Delta\mathbf{T}_a$ from the third equation of (12.60),

$$\Delta\mathbf{T}_a = \gamma\,\mathbf{K}_{TT}^{-1}\,(\mathbf{K}_{uT}^T\Delta\mathbf{u}_I + \mathbf{K}_{\omega T}^T\Delta\boldsymbol{\omega}_I), \tag{12.61}$$

which is feasible because the perturbation matrix $-(1/\gamma)\mathbf{K}_{TT}$ is nonsingular. Then, we use this $\Delta\mathbf{T}_a$ in the other two equations of eq. (12.60), which yields

$$\left(\begin{bmatrix} \mathbf{K} & \mathbf{0} \\ \mathbf{0} & \mathbf{0} \end{bmatrix} + \gamma \begin{bmatrix} \mathbf{K}_{uu} & \mathbf{K}_{u\omega} \\ \mathbf{K}_{\omega u} & \mathbf{K}_{\omega\omega} \end{bmatrix}\right) \begin{bmatrix} \Delta\mathbf{u}_I \\ \Delta\boldsymbol{\omega}_I \end{bmatrix} = \begin{bmatrix} \mathbf{p} \\ \mathbf{0} \end{bmatrix}, \tag{12.62}$$

where

$$\begin{bmatrix} \mathbf{K}_{uu} & \mathbf{K}_{u\omega} \\ \mathbf{K}_{\omega u} & \mathbf{K}_{\omega\omega} \end{bmatrix} \doteq \begin{bmatrix} \mathbf{K}_{uT}\mathbf{K}_{TT}^{-1}\mathbf{K}_{uT}^T & \mathbf{K}_{uT}\mathbf{K}_{TT}^{-1}\mathbf{K}_{\omega T}^T \\ \mathbf{K}_{\omega T}\mathbf{K}_{TT}^{-1}\mathbf{K}_{uT}^T & \mathbf{K}_{\omega T}\mathbf{K}_{TT}^{-1}\mathbf{K}_{\omega T}^T + \mathbf{K}_{\omega\omega}^{\text{stab}} \end{bmatrix}.$$

Note the similarity of this set of equations to eq. (12.45) obtained for the penalty method. Stability requires invertibility of the whole above tangent matrix.

The local Lagrange multipliers are used in our elements based on the Perturbed Lagrange method.

12.3.2 Selection of regularization parameter for drill RC

Introduction. The regularization parameter γ is used by the two methods discussed earlier, the penalty method and the Perturbed Lagrange method. The value of γ affects the solution and should ensure satisfaction of the following requirements:

1. Displacements yielded by the element with drill rotations should be identical to those yielded by an analogous element without drill rotations; this requirement is incorporated in the definition of the *extended* configuration space, see eq. (4.3).
2. For coarse meshes, displacements for the formulations with and without drill rotations are similar but not identical; the former are slightly stiffer. However, in the mesh limit, i.e. for the element's size tending to zero, the displacements should converge to the displacements of an element without drill rotations.
3. Drill rotations should converge in the mesh limit from the same side as the displacements, i.e. either from below for the fully integrated (FI) elements or from above for the reduced integrated (RI) elements.

Extreme values of γ can cause the following problems:

1. Too large values of γ can yield an ill-conditioned tangent matrix; this is a characteristic deficiency of the penalty method. The ill-conditioning is typically cured by using, instead of the penalty method, the Augmented Lagrangian method, in which the Lagrange multiplier is updated iteratively, and smaller values of γ can be used. This approach is beneficial for non-linear problems which are solved iteratively, but not for the linear ones which are solved without iterations.

   Though γ cannot be too large, it should still ensure a correct transfer of drilling rotations, see the numerical example "Bending of slender cantilever by end drilling rotation" of Sect. 12.8.2. This is an important issue but often forgotten when attention is focused on avoiding over-stiffening (locking).
2. Too small values of γ cause the tangent matrix $\mathbf{K}$ to be rank deficient. In particular, $\gamma = 0$ yields four spurious zero eigenvalues for a four-node bilinear element.

Numerical examples of Sect. 12.8.2 show that a wide range of values of γ exists for which solutions are almost constant and accurate.

Selection of the penalty value in contact mechanics. The methods of constrained optimization are widely used and tested in contact mechanics, [261, 133]. The penalty method is a basic method in this area and is used in the shortened form consisting of a single unconstrained optimization problem. Hence, selection of an optimal value of the penalty parameter requires an error analysis, which takes into account the roundoff errors and the perturbation errors due to the penalty method, see [69, 70, 157, 155].

Typically, such an analysis is limited to linear constrains such that one equation constrains displacements at some points. Note that the drill RC is more complicated, as it is a nonlinear equation involving several variables of a different type, including tangent displacements and drill rotations.

Currently, the Augmented Lagrangian method is very popular in contact mechanics and in this method the question of an optimal penalty value is less acute because smaller values of the penalty can be used, see e.g. [222].

Upper bound on the penalty parameter γ for drill RC. The theoretical considerations, which provide the bounding value of the penalty parameter γ, are given in [99], where equations of linear elasticity with a non-symmetric stress tensor are considered. For the formulation based on the potential energy, the variational problem is written in the form

$$B_\gamma(\mathbf{u}, \tilde{\boldsymbol{\psi}}; \mathbf{v}, \boldsymbol{\omega}) = \mathbf{f}(\{\mathbf{v}, \boldsymbol{\omega}\}), \qquad \forall\, \{\mathbf{v}, \boldsymbol{\omega}\} \in U, \tag{12.63}$$

where $\mathbf{u}$ is the displacement vector and $\tilde{\boldsymbol{\psi}}$ a skew symmetric tensor for an infinitesimal drilling rotation. The corresponding trial fields are denoted as $\mathbf{v}$ and $\boldsymbol{\omega}$. Besides,

$$\begin{aligned} B_\gamma(\mathbf{u}, \tilde{\boldsymbol{\psi}}; \mathbf{v}, \boldsymbol{\omega}) = &\int_\Omega (\operatorname{sym} \nabla \mathbf{v}) \cdot [\mathbb{C}\, (\operatorname{sym} \nabla \mathbf{u})]\, \mathrm{d}\Omega \\ &+ \int_\Omega (\operatorname{skew} \nabla \mathbf{v} - \boldsymbol{\omega}) \cdot \gamma (\operatorname{skew} \nabla \mathbf{u} - \tilde{\boldsymbol{\psi}})\, \mathrm{d}\Omega \end{aligned} \tag{12.64}$$

is the symmetric bilinear form and

$$\mathbf{f}(\{\mathbf{v}, \boldsymbol{\omega}\}) = \int_\Omega \mathbf{v} \cdot \mathbf{f}\, \mathrm{d}\Omega \tag{12.65}$$

is continuous. Besides, $\mathbb{C}$ is the (rank 4) constitutive tensor.

Well-posedness of a discrete variational problem depends, among the other things, on the U-ellipticity of B_γ. It requires that a constant $\eta > 0$ exists such that

$$B_\gamma(\mathbf{u}, \boldsymbol{\psi}; \mathbf{v}, \boldsymbol{\omega}) \geq \eta\, \|\{\mathbf{v}, \boldsymbol{\omega}\}\|_U^2, \qquad \forall\, \{\mathbf{v}, \boldsymbol{\omega}\} \in U, \tag{12.66}$$

where

$$\|\{\mathbf{v}, \boldsymbol{\omega}\}\|_U = \|\mathbf{v}\|_V^2 + \|\boldsymbol{\omega}\|_W^2, \qquad \forall\, \{\mathbf{v}, \boldsymbol{\omega}\} \in U,$$

$$\|\mathbf{v}\|_V^2 = \int_\Omega \|\nabla \mathbf{v}\|^2\, \mathrm{d}\Omega, \quad \forall\, \mathbf{v} \in V, \qquad \|\boldsymbol{\omega}\|_W^2 = \int_\Omega \|\boldsymbol{\omega}\|^2\, \mathrm{d}\Omega, \quad \forall\, \boldsymbol{\omega} \in W.$$

Note that $U = V \times W$, where V and W are the spaces relevant to the BVP. By using the estimation of the minimum eigenvalue of $\mathbb{C}$ for an isotropic material,

$$\min_{\varepsilon=\varepsilon^T,\,\varepsilon\neq 0} \frac{\boldsymbol{\varepsilon}\cdot(\mathbb{C}\,\boldsymbol{\varepsilon})}{\|\boldsymbol{\varepsilon}\|^2} = 2G, \tag{12.67}$$

and Korn's inequality,

$$\|\mathrm{sym}\,\nabla\mathbf{v}\|^2 \geq c_k\,\|\nabla\mathbf{v}\|^2, \tag{12.68}$$

where the constant $c_k = 1/2$ for the Dirichlet problem, we obtain

$$B_\gamma(\mathbf{v},\boldsymbol{\omega};\mathbf{v},\boldsymbol{\omega}) \geq \frac{G}{2}\|\nabla\mathbf{v}\|^2 + (G-\gamma)\|\mathrm{skew}\,\nabla\mathbf{v}\|^2 + \frac{\gamma}{2}\|\boldsymbol{\omega}\|^2. \tag{12.69}$$

Any $0 \leq \gamma \leq G$ is appropriate but the second term in the estimate vanishes for $\gamma = G$, so we obtain

$$B_\gamma(\mathbf{v},\boldsymbol{\omega};\mathbf{v},\boldsymbol{\omega}) \geq \frac{G}{2}\left(\|\nabla\mathbf{v}\|^2 + \|\boldsymbol{\omega}\|^2\right), \tag{12.70}$$

which is in accord with eq. (12.66). The value $\gamma = G$ was subsequently numerically tested in [102].

Numerical tests of our elements of Sect. 12.8.2 confirm that, generally, the value $\gamma = G$ is a good choice. However, in several situations, a modification of this value is beneficial.

Selection of value of the penalty parameter γ for drill RC. The shell finite elements are very complicated as they (i) involve a large number of variables, (ii) are non-linear, which means that problems are solved iteratively and the number of terms is very large, and (iii) are generated using a complex methodology which cannot easily be accounted for in theoretical considerations.

For this reason, theoretical predictions of the value of γ provide only a general guidance, while a reliable and practically meaningful value of γ must be the result of proper testing. To avoid repeating the process of selection of γ for each BVP, a set of suitable benchmark tests must be used. These problems are solved for a range of values of γ and for each, the segment in which the solution is accurate and almost constant is identified. The final single value of γ should be problem-independent, so we must choose the value which is correct for all benchmark tests. In

this task, plots of the obtained displacements and drilling rotations vs. γ are particularly useful.

Generally, the value of γ should account for the element's volume and the material characteristics.

1. In the weak formulation, eq. (12.35), the element volume is accounted for by integration, so the penalty number does not have to include it. But for the strong formulation of eq. (12.33), it must be explicitly included in γ.
2. The material characteristics are accounted for by linking γ to one of the eigenvalues of the constitutive matrix. For instance, for the SVK material and the plane stress conditions, the eigenvalues of the constitutive matrix $\mathbf{C}$ are given by eq. (7.78) and the smallest eigenvalue is $E/(1+\nu) = 2G$. Hence, it is reasonable to relate the value of γ to the shear modulus G.

Hence, in the weak formulation, we use the definition

$$\gamma = \epsilon\, G, \tag{12.71}$$

where ϵ is a scaling factor. In the numerical tests in Sect. 12.8.2, we select the value of ϵ.

Method of calculating γ for shells of [189]. In this work, the stiffness matrix for a single shell element is divided into parts related to displacements $\mathbf{u}$ and rotation parameters $\boldsymbol{\psi}$ as follows:

$$\mathbf{K} = \begin{bmatrix} \mathbf{K}_{uu} & \mathbf{K}_{u\psi} \\ \mathbf{K}_{\psi u} & \mathbf{K}_{\psi\psi} \end{bmatrix} \tag{12.72}$$

and only diagonal sub-matrices $\mathbf{K}_{uu}$ and $\mathbf{K}_{\psi\psi}$ are considered. They consist of the classical part (C) and the part for the drill RC (D),

$$\mathbf{K}_{uu} = \mathbf{K}^{\mathrm{C}}_{uu} + \gamma\, \mathbf{K}^{\mathrm{D}}_{uu}, \qquad \mathbf{K}_{\psi\psi} = \mathbf{K}^{\mathrm{C}}_{\psi\psi} + \gamma\, \mathbf{K}^{\mathrm{D}}_{\psi\psi}. \tag{12.73}$$

Each of the sub-matrices is considered separately and maximum absolute values of their diagonal terms are compared

$$\gamma_u = \frac{\max|\operatorname{diag}\mathbf{K}^{\mathrm{C}}_{uu}|}{\max|\operatorname{diag}\mathbf{K}^{\mathrm{D}}_{uu}|}, \qquad \gamma_\psi = \frac{\max|\operatorname{diag}\mathbf{K}^{\mathrm{C}}_{\psi\psi}|}{\max|\operatorname{diag}\mathbf{K}^{\mathrm{D}}_{\psi\psi}|}. \tag{12.74}$$

The penalty parameter is defined as

$$\gamma = \frac{1}{100}\min(\gamma_u, \gamma_\psi), \tag{12.75}$$

where the value $1/100$ was selected by numerical experiments. The value of γ is calculated only once per analysis, at the beginning, for the linear stiffness matrix.

This method relies on the fact that the diagonal terms of $\mathbf{K}_{uu}$ and $\mathbf{K}_{\psi\psi}$ are much larger than the off-diagonal ones, which allows us to avoid costly eigenvalue analyses.

12.4 EADG method for formulations with rotations

The Enhanced Assumed Displacement Gradient (EADG) method for 2D elements was discussed in Sect. 11.4.3; below it is extended to the 2D+drill elements.

Consider the two-field (2-F) functionals with rotations of Sect. 4 and denote them as $F_2(\boldsymbol{\chi}, \mathbf{Q})$. Let us rewrite eq. (11.70), defining the EADG method, as

$$\mathbf{F} \doteq \nabla\boldsymbol{\chi} + \tilde{\mathbf{H}}, \tag{12.76}$$

where $\nabla\boldsymbol{\chi} = \mathbf{I} + \nabla\mathbf{u}^{\mathrm{c}}$. In the EADG method, we add two independent fields to $F_2(\boldsymbol{\chi}, \mathbf{Q})$: the nominal stress $\mathbf{P}$ and the field $\mathbf{F}$, and construct the following 4-F functional

$$F_4(\boldsymbol{\chi}, \mathbf{Q}, \mathbf{F}, \mathbf{P}) \doteq F_2(\mathbf{Q}, \mathbf{F}) + \int_B \mathbf{P} \cdot (\nabla\boldsymbol{\chi} - \mathbf{F})\, \mathrm{d}V, \tag{12.77}$$

where $\mathbf{P}$ is a Lagrange multiplier for the formula linking $\nabla\boldsymbol{\chi}$ and the independent $\mathbf{F}$. Note that now $F_2(\mathbf{Q}, \mathbf{F})$ involves the independent $\mathbf{F}$. By using eq. (12.76), this functional becomes

$$F_4(\boldsymbol{\chi}, \mathbf{Q}, \tilde{\mathbf{H}}, \mathbf{P}) = F_3(\boldsymbol{\chi}, \mathbf{Q}, \tilde{\mathbf{H}}) + \int_B \mathbf{P} \cdot \tilde{\mathbf{H}}\, \mathrm{d}V, \tag{12.78}$$

in which we have the enhancing $\tilde{\mathbf{H}}$. If the enhancing $\tilde{\mathbf{H}}$ is orthogonal to the stress, i.e. $\int_B \mathbf{P} \cdot \tilde{\mathbf{H}}\, \mathrm{d}V = 0$, then the last term of eq. (12.78) vanishes and we obtain the 3-F functional

$$F_3(\boldsymbol{\chi}, \mathbf{Q}, \tilde{\mathbf{H}}), \tag{12.79}$$

which does not depend on $\mathbf{P}$ and is used in the element's implementation.

In this way we can obtain the 3-F enhanced functionals for particular forms of $F_2(\boldsymbol{\chi}, \mathbf{Q})$. For instance, for the functionals $\tilde{F}_2^{\mathrm{2PK}}(\boldsymbol{\chi}, \mathbf{Q})$ of eq. (4.73) and $F_2^{**}(\boldsymbol{\chi}, \mathbf{Q})$ of eq. (4.77), we obtain

$$\tilde{F}_3^{\mathrm{2PK}}(\boldsymbol{\chi}, \tilde{\mathbf{H}}, \mathbf{Q}) \doteq$$
$$\int_B \left\{ \mathcal{W}\left[(\nabla\boldsymbol{\chi} + \tilde{\mathbf{H}})^T (\nabla\boldsymbol{\chi} + \tilde{\mathbf{H}}) \right] + F_{\mathrm{RC}}(\boldsymbol{\chi}, \tilde{\mathbf{H}}, \mathbf{Q}) \right\} \mathrm{d}V - F_{\mathrm{ext}}, \quad (12.80)$$
$$F_3^{**}(\boldsymbol{\chi}, \tilde{\mathbf{H}}, \mathbf{Q}) \doteq$$
$$\int_B \left\{ \mathcal{W}\left[\mathbf{Q}^T (\nabla\boldsymbol{\chi} + \tilde{\mathbf{H}}) \right] + F_{\mathrm{RC}}(\boldsymbol{\chi}, \tilde{\mathbf{H}}, \mathbf{Q}) \right\} \mathrm{d}V - F_{\mathrm{ext}}, \quad (12.81)$$

where the RC term has the penalty form

$$F_{\mathrm{RC}}(\boldsymbol{\chi}, \tilde{\mathbf{H}}, \mathbf{Q}) \doteq \frac{\gamma}{2} \mathrm{skew}[\mathbf{Q}^T (\nabla\boldsymbol{\chi} + \tilde{\mathbf{H}})] \cdot \mathrm{skew}[\mathbf{Q}^T (\nabla\boldsymbol{\chi} + \tilde{\mathbf{H}})]. \quad (12.82)$$

The RC term is also enhanced by $\tilde{\mathbf{H}}$, which is not possible within the EAS method. These functionals were used in [255].

Modification of the EADG method motivated by the EAS method. The EAS method has a certain advantage over the EADG method in non-linear 2D problems, i.e. is slightly faster and converges better. The enhancement of $\mathbf{F}$ is needed in the drill RC equation, so it should be retained in its original form, but we can simplify the Cauchy–Green deformation tensor $\mathbf{C}$ to a form which is similar to that implied by the EAS method.

1. For the EAS method, see eq. (11.62), the enhanced Cauchy–Green tensor is

$$\mathbf{C} \doteq \mathbf{F}^T\mathbf{F} + \mathbf{G}^\xi, \qquad \mathbf{G}^\xi \doteq \begin{bmatrix} q_1\xi & q_3\xi + q_4\eta \\ q_3\xi + q_4\eta & q_2\eta \end{bmatrix}, \quad (12.83)$$

   where, for simplicity, we omitted the Jacobians.
2. In the EADG method, the enhancing modes are added to the deformation gradient, see eq. (12.76), and the Cauchy–Green deformation tensor is

$$\mathbf{C} = \mathbf{F}^T\mathbf{F} + \mathbf{F}^T\tilde{\mathbf{H}} + \tilde{\mathbf{H}}^T\mathbf{F} + \tilde{\mathbf{H}}^T\tilde{\mathbf{H}}. \quad (12.84)$$

   Let us use the EADG4 enhancement of eq. (11.71) in which, for simplicity, we omit the Jacobians. Then, we have

$$\tilde{\mathbf{H}} = \begin{bmatrix} \xi\, q_1 & \eta\, q_3 \\ \xi\, q_4 & \eta\, q_2 \end{bmatrix}, \qquad \mathbf{F} = \begin{bmatrix} F_{11} & F_{12} \\ F_{21} & F_{22} \end{bmatrix} \quad (12.85)$$

and the last three components of eq. (12.84) involve the enhancement and are

$$\mathbf{F}^T\tilde{\mathbf{H}} = \begin{bmatrix} r_1\,\xi & r_3\,\eta \\ r_4\,\xi & r_2\,\eta \end{bmatrix}, \quad \tilde{\mathbf{H}}^T\mathbf{F} = \begin{bmatrix} r_1\,\xi & r_4\,\xi \\ r_3\,\eta & r_2\,\eta \end{bmatrix}, \quad \tilde{\mathbf{H}}^T\tilde{\mathbf{H}} = \begin{bmatrix} r_5\,\xi^2 & r_7\,\eta\xi \\ \text{sym.} & r_6\,\eta^2 \end{bmatrix},$$

where the coefficients $r_i \quad (i = 1, \ldots, 7)$ do not depend on ξ and η. The structure of these three components can be compared with the structure of $\mathbf{G}^\xi$ for the EAS method of eq. (12.83):

a) the sum

$$\mathbf{F}^T\tilde{\mathbf{H}} + \tilde{\mathbf{H}}^T\mathbf{F} = \begin{bmatrix} 2r_1\xi & r_3\xi + r_4\eta \\ r_3\xi + r_4\eta & 2r_2\eta \end{bmatrix} \tag{12.86}$$

has a similar structure as the $\mathbf{G}^\xi$ enhancement of the EAS method, i.e. the diagonal terms are linear (and incomplete) in either ξ or η, while the off-diagonal terms are sums of linear terms in ξ and η.

b) the component $\tilde{\mathbf{H}}^T\tilde{\mathbf{H}}$ contains terms of a higher order than those in eq. (12.83) for the EAS method and, hence, this term can be safely omitted from eq. (12.84).

The above modifications make the element slightly faster, and slightly stiffer, but the difference is small. For instance, in Cook's tapered panel example of Sect. 15.2.7, the difference in the displacement and drill rotation of the tip is $< 0.2\%$.

Finally, note that we can also consider the following simplification:

$$\mathbf{F}^T\tilde{\mathbf{H}} + \tilde{\mathbf{H}}^T\mathbf{F} \approx \tilde{\mathbf{H}} + \tilde{\mathbf{H}}^T = \begin{bmatrix} 2q_1\xi & q_3\xi + q_4\eta \\ q_3\xi + q_4\eta & 2q_2\eta \end{bmatrix}, \tag{12.87}$$

and then similarity to the $\mathbf{G}^\xi$ enhancement of the EAS method is even closer. However, this version does not work well in the twisted ring example of Sect. 15.3.15.

12.5 Mixed HW and HR functionals with rotations

HW functionals with rotations. Consider the classical form of the 3-F Hu–Washizu (HW) functional of eq. (11.1). To obtain the HW functional with rotations, the Lagrange multiplier method is applied to eq. (11.1), which yields the five-field functional

$$F_{\mathrm{HW5}}(\mathbf{u},\mathbf{Q},\boldsymbol{\sigma},\boldsymbol{\varepsilon},\mathbf{T}_a) \doteq$$
$$\int_B \left\{\mathcal{W}(\boldsymbol{\varepsilon}) + \boldsymbol{\sigma}\cdot[\mathbf{E}(\nabla\mathbf{u}) - \boldsymbol{\varepsilon}] + \mathbf{T}_a \cdot \mathrm{skew}(\mathbf{Q}^T\mathbf{F})\right\} \mathrm{d}V - F_{\mathrm{ext}}, \quad (12.88)$$

where $\mathbf{T}_a \doteq \mathrm{skew}(\mathbf{Q}^T\mathbf{F}\mathbf{S})$ is the Lagrange multiplier for the RC equation. Two functionals derived from eq. (12.88) are particularly useful.

A. the 4-F functional, obtained by regularization of eq. (12.88) in $\mathbf{T}_a$, and elimination of $\mathbf{T}_a$,

$$\tilde{F}_{\mathrm{HW4}}(\mathbf{u},\boldsymbol{\sigma},\boldsymbol{\varepsilon},\mathbf{Q}) \doteq$$
$$\int_B \left\{\mathcal{W}(\boldsymbol{\varepsilon}) + \boldsymbol{\sigma}\cdot[\mathbf{E}(\nabla\mathbf{u}) - \boldsymbol{\varepsilon}\right\} + F_{\mathrm{RC}}^{\mathrm{P}}(\nabla\mathbf{u},\mathbf{Q})\big] \,\mathrm{d}V - F_{\mathrm{ext}}, \quad (12.89)$$

where the RC term has the penalty (P) form of eqs. (12.42) and (12.43).

B. the 5-F functional obtained by regularization of eq. (12.88) in $\mathbf{T}_a$,

$$\tilde{F}_{\mathrm{HW5}}(\mathbf{u},\mathbf{Q},\boldsymbol{\sigma},\boldsymbol{\varepsilon},\mathbf{T}_a) \doteq$$
$$\int_B \left\{\mathcal{W}(\boldsymbol{\varepsilon}) + \boldsymbol{\sigma}\cdot[\mathbf{E}(\nabla\mathbf{u}) - \boldsymbol{\varepsilon}] + F_{\mathrm{RC}}^{\mathrm{PL}}(\nabla\mathbf{u},\mathbf{Q},\mathbf{T}_a)\right\} \mathrm{d}V - F_{\mathrm{ext}}, \quad (12.90)$$

where the RC term has the perturbed Lagrange (PL) form of eqs. (12.53) and (12.55).

HR functionals with rotations. Let us take the above HW functionals with rotations and apply the same procedure which was used to obtain the Hellinger–Reissner functionals of eqs. (11.4) and (11.7). Then we obtain the HR functionals with rotations applicable to linear elastic materials.

A. From the 4-F functional of eq. (12.89), we obtain

$$\tilde{F}_{\mathrm{HR3}}(\mathbf{u},\mathbf{Q},\boldsymbol{\sigma}) \doteq$$
$$\int_B \left[-\tfrac{1}{2}\boldsymbol{\sigma}\cdot(\mathbb{C}^{-1}\boldsymbol{\sigma}) + \boldsymbol{\sigma}\cdot\mathbf{E}(\nabla\mathbf{u}) + F_{\mathrm{RC}}^{\mathrm{P}}(\nabla\mathbf{u},\mathbf{Q})\right] \mathrm{d}V - F_{\mathrm{ext}}, \quad (12.91)$$

where the penalty (P) form of the RC is given by eqs. (12.42) and (12.43).

B. From the 5-F functional of eq. (12.90), we obtain

$$\tilde{F}_{\mathrm{HR4}}(\mathbf{u},\mathbf{Q},\boldsymbol{\sigma},\mathbf{T}_a) \doteq$$
$$\int_B \left[-\tfrac{1}{2}\boldsymbol{\sigma}\cdot(\mathbb{C}^{-1}\boldsymbol{\sigma}) + \boldsymbol{\sigma}\cdot\mathbf{E}(\nabla\mathbf{u}) + F_{\mathrm{RC}}^{\mathrm{PL}}(\nabla\mathbf{u},\mathbf{Q},\mathbf{T}_a)\right] \mathrm{d}V - F_{\mathrm{ext}}, \quad (12.92)$$

where the perturbed Lagrange (PL) form of the RC term is given by eqs. (12.53) and (12.55).

For non-linear materials, we use the incremental forms of the above HW and HR functionals, obtained for the increments of displacements, stress and strain of eq. (11.5).

EADG method for HW and HR functionals. In Sect. 12.4, we described the EADG method for the 3D potential energy functionals with rotations derived in Sect. 4; for the HW and HR functionals with rotations, the procedure is simpler.

For the HW and HR functionals, the EADG method can be incorporated without using additional independent fields $\mathbf{P}$ and $\mathbf{F}$ and the term $\int_B \mathbf{P}\cdot(\nabla\boldsymbol{\chi}-\mathbf{F})\,\mathrm{d}V$, which was used in eq. (12.77). This is because we already have the independent fields $\boldsymbol{\sigma}$ and $\boldsymbol{\varepsilon}$ and the term $\int_B \boldsymbol{\sigma}\cdot(\mathbf{E}(\nabla\mathbf{u})-\boldsymbol{\varepsilon})\,\mathrm{d}V$, which can be used instead. Hence, it suffices to replace $\nabla\mathbf{u}$ by $\nabla\mathbf{u}+\tilde{\mathbf{H}}$ in $\mathbf{E}(\nabla\mathbf{u})$, which is in accord with eq. (12.76). We note that the orthogonality of stress and the enhancing field is not required.

The EADG enhancement is applied to the HW functionals with rotations of eqs. (12.89) and (12.90), and the HR functionals with rotations of eqs. (12.91) and (12.92).

12.6 2D+drill elements for bilinear shape functions

The characteristics of each 2D+drill four-node element (with the drilling rotation), which are presented below, consists of three parts:

1. the designation of the plane (2D) four-node element (without the drilling rotation) of Sect. 11, which is being extended by inclusion of the drilling rotation,
2. the specification of the mixed functional on which the element is based,
3. the description of the treatment of the functional for the drill RC, F_{RC}. The weak (integral) forms of the drill RC was used; the penalty method is implemented as specified in Table 12.4, while the Perturbed Lagrange method as specified in Table 12.5.

12.6.1 EADG4 elements based on potential energy

The elements characterized below have two features: (i) they extend the EADG4 element without the drilling rotation of Sect. 11.4.3 and (ii) are

Table 12.4 Implementation of the penalty method (**P**) for drill RC.

1. weak (integral) form of drill RC, as in eq. (12.35), functional $F_{\rm RC}$ of eq. (12.42),
2. expansion of $\mathbf{Q}^T\mathbf{F}$ product of eq. (12.27), for which drill RC is given by eq. (12.28),
3. stabilization of spurious mode of eq. (12.25).

Table 12.5 Implementation of the Perturbed Lagrange method (**PL**) for drill RC.

1. weak (integral) form of drill RC, as in eq. (12.36), functional $F_{\rm RC}$ of eq. (12.53), Lagrange multiplier tensor of eq. (12.56) and representation of eq. (12.57).
2. expansion of $\mathbf{Q}^T\mathbf{F}$ product of eq. (12.27), for which drill RC is given by eq. (12.28),
3. stabilization of spurious mode of eq. (12.25).

based on the potential energy functional with rotations of eq. (4.73). Two elements were selected:

1. **Element EADG4+P**, which has the following features:
   a) the penalty method is implemented as specified in Table 12.4,
   b) it uses four additional parameters, the multipliers of the EADG modes.
2. **Element EADG4+PL**, which has the following features:
   a) the Perturbed Lagrange method is implemented as specified in Table 12.5,
   b) it uses seven additional parameters: four multipliers of the EADG modes and three parameters of the Lagrange multiplier.

As show the numerical tests, these 2D+drill elements perform very well for coarse distorted meshes, despite a small number of parameters. In nonlinear tests, the second (PL) element has a larger radius of convergence.

12.6.2 Assumed stress HR5-S elements

The elements characterized below are based on the HR functionals with rotations of eqs. (12.91) and (12.92). Their 2D counterparts were described in Sect. 11.5.1. The same five-parameter representation of eq. (11.126) is used for stress. No enhancement is applied.

1. **Element HR5-S+P** which has the following features:
   a) the penalty method is implemented as specified in Table 12.4,
   b) it uses five additional parameters, which are multipliers of the stress modes.
2. **Element HR5-S+PL** which has the following features:
   a) the Perturbed Lagrange method is implemented as specified in Table 12.5,
   b) it uses eight additional parameters: five multipliers of the stress modes and three parameters of the Lagrange multiplier.

As show the numerical tests, these 2D+drill elements are worse for coarse distorted meshes than, e.g., the EADG4 element. They show a substantial decrease of accuracy, comparing to their 2D counterparts.

12.6.3 Assumed stress/enhanced strain HR7-S elements

A poor performance of the 2D+drill HR elements based on the five-parameter representation of stresses caused that we considered the seven-parameter representation of stresses and the strain enhancement. No such 2D elements are described in Sect. 11.5 because they perform identically to the HR5-S element but use more modes, so are less effective.

The assumed stress/enhanced strain elements are based on the HR functionals of eqs. (12.91) and (12.92) additionally enhanced, by replacing $\nabla\mathbf{u}$ by $\nabla\mathbf{u}+\tilde{\mathbf{H}}$, as described in Sect. 12.5. In these functionals, $\mathbf{u}$, $\mathbf{Q}$ are the compatible fields, while $\boldsymbol{\sigma}$, $\boldsymbol{\varepsilon}$, $\mathbf{T}_a$, $\tilde{\mathbf{H}}$ are the assumed fields. Besides,

1. the assumed stress and the increment of the assumed stress are constructed as follows:

$$\boldsymbol{\sigma}^a = \mathbf{J}_c\ \boldsymbol{\sigma}^\xi\ \mathbf{J}_c^T, \qquad \Delta\boldsymbol{\sigma}^a = \mathbf{J}_c\ \Delta\boldsymbol{\sigma}^\xi\ \mathbf{J}_c^T, \tag{12.93}$$

   which is the transformation rule for the contravariant components of a tensor of eq. (11.124), and $\boldsymbol{\sigma}^\xi$ contains the seven-parameter representation in terms of the skew coordinates

$$\boldsymbol{\sigma}^\xi \doteq \begin{bmatrix} q_1 + q_2\, y_S & q_5 + q_6\, x_S + q_7\, y_S \\ \text{sym.} & q_3 + q_4\, x_S \end{bmatrix}. \tag{12.94}$$

   Besides, $\Delta\boldsymbol{\sigma}^\xi$ has a structure of $\boldsymbol{\sigma}^\xi$, with the multipliers q_i replaced by Δq_i.

2. The EADG enhancement of eq. (11.71) is used in the form

$$\tilde{\mathbf{H}}_g \doteq \mathbf{J}_c \, \mathbf{G}_g^{\xi} \, \mathbf{J}_c^{-1} \begin{pmatrix} j_c \\ j_g \end{pmatrix}, \qquad \mathbf{G}^{\xi} \doteq \begin{bmatrix} 0 & \eta \, q_8 \\ \xi \, q_9 & 0 \end{bmatrix}, \tag{12.95}$$

where the EADG2 representation involves two parameters.

Two elements were developed:

1. **Element HR7+EADG2+P** which has the following features:
   a) the penalty method is implemented as specified in Table 12.4,
   b) it uses nine additional parameters: seven multipliers of stress modes and two multipliers of the EADG enhancement.
2. **Element HR7+EADG2+PL** which has the following features:
   a) the Perturbed Lagrange method is implemented as specified in Table 12.5,
   b) it uses 12 additional parameters; nine parameters identical as in the previous element, and three parameters of the Lagrange multiplier.

As show the numerical tests, the above elements perform very well for coarse distorted meshes, better than the EADG4 element. In non-linear tests, the second (PL) element has a much larger radius of convergence.

Remark. Note that we can also consider a different seven-parameter representation

$$\boldsymbol{\sigma}^{\xi} \doteq \begin{bmatrix} q_1 + q_2 \, y_S + q_6 \, x_S & q_5 - q_7 \, x_S - q_6 \, y_S \\ \text{sym.} & q_3 + q_4 \, x_S + q_7 \, y_S \end{bmatrix}, \tag{12.96}$$

where some parameters are repeated in the diagonal and off-diagonal terms. This representation was used in several earlier papers on mixed (or hybrid) methods; (i) in Cartesian coordinates in [223] and (ii) in oblique coordinates in [184]. More recently, it was also used in [265, 177], but in different forms; the relation between these forms was established in [256], eqs. (38) and (41).

Both these seven-parameter representations are equally good for the 2D elements, but for the 2D+drill elements, the representation (12.96) is slightly worse and, for this reason, is not used here.

12.6.4 Assumed stress and strain HW14-SS elements

The elements characterized below are based on the non-enhanced HW functionals with rotations of eq. (12.89) or eq. (12.90). Their 2D counterparts were described in Sect. 11.5.2.

1. **Element HW14-SS+P** which has the following features:
   a) the penalty method is implemented as specified in Table 12.4,
   b) it uses 14 additional parameters: five multipliers of the stress modes of eq. (11.126), and nine multipliers of the strain modes of eq. (11.140).
2. **Element HW14-SS+PL** which has the following features:
   a) the Perturbed Lagrange method is implemented as specified in Table 12.5.
   b) it uses 17 additional parameters: fourteen parameters identical as in the previous element, and three parameters of the Lagrange multiplier.

As show the numerical tests, these 2D+drill elements are worse for coarse distorted meshes than, e.g., the EADG4 element. They show a substantial decrease of accuracy compared to their 2D counterparts.

12.6.5 Assumed stress and strain/enhanced strain HW18-SS elements

A poor performance of the 2D+drill HW elements based on five-parameter representation of stress caused that we considered the seven-parameter representation of stresses and the strain enhancement. No 2D elements of this type are described in Sect. 11.5 because they perform identically to the HW14-S element but are less effective, as they use more modes.

The assumed stress and strain/enhanced strain elements characterized below are based on the HW functionals with rotations of eqs. (12.89) or (12.90) additionally enhanced, by replacing $\nabla\mathbf{u}$ by $\nabla\mathbf{u} + \tilde{\mathbf{H}}$, as described in Sect. 12.5. In these functionals, $\mathbf{u}$, $\mathbf{Q}$ are the compatible fields, while $\boldsymbol{\sigma}$, $\boldsymbol{\varepsilon}$, $\mathbf{T}_a$, $\tilde{\mathbf{H}}$ are the assumed fields. Besides,

1. the assumed stress and the increment of the assumed stress are constructed as follows:

$$\boldsymbol{\sigma}^a = \mathbf{J}_c\, \boldsymbol{\sigma}^\xi\, \mathbf{J}_c^T, \qquad \Delta\boldsymbol{\sigma}^a = \mathbf{J}_c\, \Delta\boldsymbol{\sigma}^\xi\, \mathbf{J}_c^T, \tag{12.97}$$

   which is the transformation rule for the contravariant components of a tensor of eq. (11.124) and $\boldsymbol{\sigma}^\xi$ contains the seven-parameter representation in terms of the skew coordinates

$$\boldsymbol{\sigma}^\xi \doteq \begin{bmatrix} q_1 + q_2\, y_S & q_5 + q_6\, x_S + q_7\, y_S \\ \text{sym.} & q_3 + q_4\, x_S \end{bmatrix}. \tag{12.98}$$

   Besides, $\Delta\boldsymbol{\sigma}^\xi$ has a structure of $\boldsymbol{\sigma}^\xi$ but with q_i replaced by Δq_i.

2. The assumed strain is constructed as

$$\boldsymbol{\varepsilon}^a = \mathbf{J}_c^{-T}\ \boldsymbol{\varepsilon}_\xi\ \mathbf{J}_c^{-1}, \tag{12.99}$$

using the transformation rule of eq. (11.139) for the covariant components of a tensor. The nine-parameter strain representation of $\boldsymbol{\varepsilon}_\xi$ is given by eq. (11.140), i.e.

$$\boldsymbol{\varepsilon}_\xi \doteq \begin{bmatrix} q_8 + q_9\, y_S + q_{10}\, x_S & q_{14} + q_{15}\, x_S + q_{16}\, y_S \\ \text{sym.} & q_{11} + q_{12}\, x_S + q_{13}\, y_S \end{bmatrix}. \tag{12.100}$$

3. The gradient of displacements is enhanced as follows:

$$\nabla \mathbf{u} \doteq \nabla \mathbf{u}^c + \tilde{\mathbf{H}}, \tag{12.101}$$

where $\nabla \mathbf{u}^c$ is the gradient of compatible displacements and $\tilde{\mathbf{H}}$ is the assumed enhancing field constructed as follows using the EADG method:

$$\tilde{\mathbf{H}}_g = \mathbf{J}_c\ \mathbf{G}_g\ \mathbf{J}_c^{-1} \begin{pmatrix} j_c \\ j_g \end{pmatrix}, \qquad \mathbf{G} = \begin{bmatrix} 0 & y_S\, q_{17} \\ x_S\, q_{18} & 0 \end{bmatrix}, \tag{12.102}$$

where g indicates the Gauss point.

Two elements were developed:

1. **Element HW18-SS+EADG2+P** which has the following features:
   a) the penalty method is implemented as specified in Table 12.4,
   b) it uses 18 additional parameters: seven multipliers of the stress modes, nine multipliers of the strain modes, and two parameters of the EADG2 enhancement.
2. **Element HW18-SS+EADG2+PL** which has the following features:
   a) the Perturbed Lagrange method is implemented as specified in Table 12.5.
   b) it uses 21 additional parameters: 18 parameters identical as in the previous element, and three parameters of the Lagrange multiplier.

As show the numerical results of linear tests, e.g. of Table 12.6, the above elements with drilling rotation

1. perform identically to the HR7-S+EADG2 elements with the drilling rotation. Thus, the equivalence of linear HR and HW 2D elements established in [257] is maintained by the present 2D+drill formulation.
2. Perform very well for coarse distorted meshes, better than the EADG4 element.

12.7 2D+drill elements for Allman shape functions

Historical note. The Allman shape functions were first successfully applied to 2D triangles in [1, 27] and later extrapolated to 2D quadrilaterals in [55], where a procedure of transforming an eight-node serendipity element to a four-node element with nodal drilling rotations was proposed. This procedure is commonly used in Allman-type quadrilaterals, although it needs to be modified for large drilling rotations.

At first, the Allman shape functions were treated as a way to improve accuracy of low-order elements. Soon their ability to incorporate the drilling rotation was appreciated; this was before the role of the RC equation was recognized. The Allman shape functions can be applied in two types of four-node elements:

1. 2D+drill elements. In [144] Table 1, it is stressed that such elements are eight times faster than, e.g., eight-node elements without drilling dofs, with only slightly less accuracy in small strain problems.
2. Shell elements, where the presence of the drilling rotation in the membrane part is an advantage, as it allows us to use a three-parameter representation of rotations and to treat all rotational dofs in the same way.

An overview of the works on four-node quadrilaterals based on the Allman shape functions is given in [255] and it includes such papers as [117, 113, 235, 144, 109, 112, 87, 203]. This overview provided the motivation for the formulation which generalizes the Allman shape functions to handle large rotations and uses the EADG enhancement.

12.7.1 Allman-type shape functions

The Allman-type shape functions for a quadrilateral element are obtained by the procedure, which has two characteristic features:

1. the hierarchical shape functions are used for displacements of an eight-node 2D element,
2. the hierarchical mid-side displacements are expressed by corner drilling rotations,

which means that the element displacements become functions of corner displacements and corner drilling rotations, i.e.

$$\underbrace{\mathbf{u}(\xi,\eta,\ \mathbf{u}_I)}_{\text{8-node, 2D}} = \underbrace{\mathbf{u}(\xi,\eta,\ \mathbf{u}_I,\omega_I)}_{\text{4-node, 2D+drill}}, \qquad I=1,2,3,4. \tag{12.103}$$

Hierarchical shape functions for displacements of 2D quadrilateral. The displacements of the eight-node 2D quadrilateral of Fig. 12.4 can be approximated as follows:

$$\mathbf{u}(\xi,\eta) = \sum_{I=1}^{4} N_I(\xi,\eta)\ \mathbf{u}_I + \sum_{H=5}^{8} N_H(\xi,\eta)\ \Delta\mathbf{u}_H, \tag{12.104}$$

where $N_I(\xi,\eta)$ are the standard bilinear shape functions of eq. (10.3), and $N_H(\xi,\eta)$ are the hierarchical shape functions, defined as

$$\begin{aligned} N_5(\xi,\eta) &= \tfrac{1}{2}(1-\xi^2)(1-\eta), \qquad & N_7(\xi,\eta) &= \tfrac{1}{2}(1-\xi^2)(1+\eta), \\ N_6(\xi,\eta) &= \tfrac{1}{2}(1-\eta^2)(1+\xi), \qquad & N_8(\xi,\eta) &= \tfrac{1}{2}(1-\eta^2)(1-\xi). \end{aligned} \tag{12.105}$$

Note that $\mathbf{u}_I$ are the nodal displacement vectors, while $\Delta\mathbf{u}_H$ are the hierarchical displacement vectors at mid-points of the element boundaries, see Fig. 12.7.

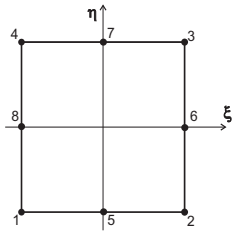

Fig. 12.4 Numeration of nodes of eight-node element.

The shape functions for a selected mid-side node of the hierarchical eight-node element and the Lagrange nine-node element are shown in Fig. 12.5. More details on the differences between these two families of shape functions can be found, e.g., in [268] Chap. 8.

To express the hierarchical displacement $\Delta\mathbf{u}_H$ in eq. (12.104) in terms of nodal drilling rotations ω_I, we consider a single boundary of a quadrilateral element and treat it as a beam. Note that

1. In the classical Allman formula, only one component of $\Delta\mathbf{u}_H$ is linked with the nodal drilling rotations, this one which is normal to the beam. Hence, this formula is valid only for small drilling rotations.
2. For large drilling rotations, the form of the Allman approximations involving two components of $\Delta\mathbf{u}_H$ must be used and was derived in [255]. Another possibility is to use the incremental formulation, but this precludes the straightforward use of automatic differentiation.

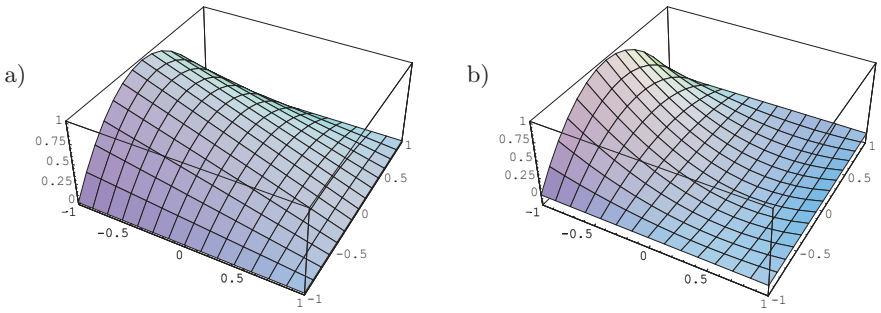

Fig. 12.5 A shape function for a mid-side node of: a) hierarchical eight-node element, b) Lagrangian nine-node element.

Classical Allman shape functions. To determine the mid-side hierarchical displacement $\Delta\mathbf{u}_I$ in eq. (12.104), we select one boundary of a quadrilateral, e.g. defined by nodes 1-5-2, and further consider a planar beam along it, see Fig. 12.6.

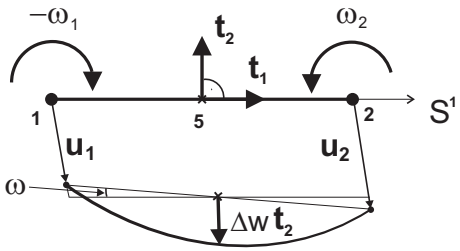

Fig. 12.6 Classical Allman shape functions: small rotation of a selected boundary.

When the rotation ω is small, then the normal displacement component u_2 is much bigger than the tangent component u_1 and we may write

$$\mathbf{u} \approx w\,\mathbf{t}_2, \tag{12.106}$$

where $w \doteq u_2$ is the normal displacement and $\mathbf{t}_2$ is a vector normal to the boundary, and a director of the beam.

Let us define the shape functions for the beam,

$$M_1(\xi) \doteq \tfrac{1}{2}(1-\xi), \quad M_2(\xi) \doteq \tfrac{1}{2}(1+\xi), \quad M_0(\xi) \doteq 1-\xi^2, \tag{12.107}$$

where $M_1(\xi)$ and $M_2(\xi)$ are linear functions and $M_0(\xi)$ is a bubble function. The rotation and the normal displacement are approximated as

$$\omega(\xi) = M_1(\xi)\,\omega_1 + M_2(\xi)\,\omega_2,$$
$$w(\xi) = M_1(\xi)\,w_1 + M_2(\xi)\,w_2 + M_0(\xi)\,\Delta w, \qquad (12.108)$$

where $M_0(\xi)$ multiplies the hierarchical mid-side displacement Δw. Note that ω_1, ω_2 and w_1, w_2 are the nodal values, while Δw is unknown. However, Δw can be linked with the nodal rotations as follows.

To calculate the hierarchical mid-side displacement Δw, we use the condition related to the transverse shear strain ε_{12} of the beam,

$$(\varepsilon_{12,\xi})|_{\xi=0} = 0, \qquad (12.109)$$

i.e. we set to zero the first derivative of the shear strain at the mid-point of the edge.

The transverse shear strain of the beam undergoing small rotations is defined as

$$\varepsilon_{12} = -\omega + w_{,1}, \qquad (12.110)$$

where $(\ )_{,1} \doteq \partial/\partial S^1$, and S^1 is the arc-length coordinate in the direction $\mathbf{t}_1$. Hence, $(\ )_{,1} = (1/L)(\ )_{,\xi}$, where L is the length of the boundary. For the approximations of eq. (12.108), the transverse shear strain becomes

$$\varepsilon_{12}(\xi,\eta) = \frac{1}{L}(w_2 - w_1 - 4\Delta w\,\xi) + M_1(\xi)\,\omega_1 + M_2(\xi)\,\omega_2, \qquad (12.111)$$

from which, using the condition (12.109), we obtain

$$\Delta w = -\frac{L}{8}\,(\omega_2 - \omega_1). \qquad (12.112)$$

This is the classical formula for the hierarchical mid-side normal displacement. Then we can write the vector of hierarchical mid-side displacement for all boundaries as follows:

$$\Delta\mathbf{u}_H \doteq -\frac{L_{JK}}{8}\,(\omega_K - \omega_J)\,\mathbf{n}_{JK}, \qquad H = 5,6,7,8, \qquad (12.113)$$

where $J = H - 4$, $K = \mathrm{mod}(H,4) + 1$, and L_{JK} is the length of the boundary JK. Here, $\mathbf{n}_{JK}$ is the vector normal to the **initial** element boundary. This formula can be directly used in eq. (12.104), which then depends only on nodal displacements and on nodal drilling rotations.

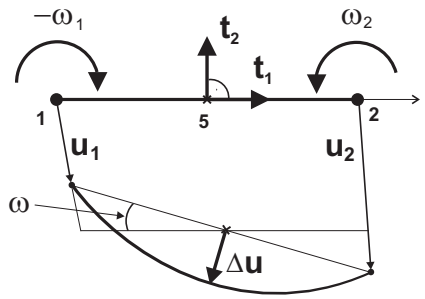

Fig. 12.7 Allman shape functions for large rotations of a selected boundary.

Allman-type shape functions for finite drilling rotation. To determine the mid-side hierarchical displacement $\Delta\mathbf{u}_I$ in eq. (12.104), we select one boundary of a quadrilateral, e.g. defined by nodes 1-5-2, and consider a planar beam along it, see Fig. 12.7.

When the rotation ω is large we have to account for both components of the displacement vectors,

$$\mathbf{u} = u_1\,\mathbf{t}_1 + u_2\,\mathbf{t}_2. \tag{12.114}$$

To calculate the hierarchical mid-side displacement $\Delta\mathbf{u}$, we can use two conditions related to the transverse shear strain ε_{12} of the beam,

$$(\varepsilon_{12,\xi})|_{\xi=0} = 0, \qquad (\varepsilon_{12,\xi\xi})|_{\xi=0} = 0, \tag{12.115}$$

i.e. we set to zero the first and the second derivatives of the shear strain at the mid-point of the edge. These conditions were proposed in [255].

The transverse shear strain of a beam undergoing large rotations is defined as

$$\varepsilon_{12} \doteq \tfrac{1}{2}\mathbf{x}_{,1}\cdot\mathbf{a}_2, \tag{12.116}$$

where $\mathbf{x}$ is the current position vector and the current director is $\mathbf{a}_2 \doteq \mathbf{Q}\,\mathbf{t}_2$, where $\mathbf{Q}$ is the drilling rotation tensor. For small rotations and $\mathbf{t}_{1,1} = \mathbf{t}_{2,1} \approx \mathbf{0}$, eq. (12.116) yields the transverse shear strain of eq. (12.110). However, in the derivation which follows, the magnitude of rotations is not restricted.

For this reason, instead of the approximation of the normal displacement component w we approximate the whole displacement vector

$$\mathbf{u}(\xi) = M_1(\xi)\,\mathbf{u}_1 + M_2(\xi)\,\mathbf{u}_2 + M_0(\xi)\,\Delta\mathbf{u}, \tag{12.117}$$

where $\Delta\mathbf{u}$ is the hierarchical mid-side displacement vector. The drilling rotation $\omega(\xi)$ is approximated as in eq. (12.108).

We apply these approximations to particular terms of the transverse shear strain of eq. (12.116), and then separate the constant terms, indicated by "0", and the terms depending on ξ, in the following way:

1. The derivative of the current position vector is $\mathbf{x}_{,1} = (\mathbf{y} + \mathbf{u})_{,1} = \mathbf{t}_1 + \mathbf{u}_{,1}$, thus for the assumed shape functions, we obtain

$$\mathbf{u}_{,1} = \frac{2}{L}\mathbf{u}_{,\xi} = \frac{2}{L}\mathbf{u}^0_{,\xi} + \frac{2}{L}\Delta\mathbf{u}(-2\xi), \tag{12.118}$$

   where $\mathbf{u}^0_{,\xi} \doteq \frac{1}{2}(\mathbf{u}_2 - \mathbf{u}_1)$ is the constant part of $\mathbf{u}_{,\xi}$ and L is the side length.
2. The forward rotated director is expressed as $\mathbf{a}_2 \doteq \mathbf{Q}_0\mathbf{t}_2 = c\,\mathbf{t}_2 - s\,\mathbf{t}_1$, where the drilling rotation tensor $\mathbf{Q} = c\,(\mathbf{t}_1\otimes\mathbf{t}_1 + \mathbf{t}_2\otimes\mathbf{t}_2) + s\,(\mathbf{t}_2\otimes\mathbf{t}_1 - \mathbf{t}_1\otimes\mathbf{t}_2)$, $s \doteq \sin\omega$ and $c \doteq \cos\omega$. For the assumed shape functions $\omega(\xi) = \omega_0 + \xi\,\omega_{,\xi}$ and we obtain

$$\begin{aligned} s &= \sin(\omega_0 + \xi\,\omega_{,\xi}) = s_0\cos(\xi\,\omega_{,\xi}) + c_0\sin(\xi\,\omega_{,\xi}),\\ c &= \cos(\omega_0 + \xi\,\omega_{,\xi}) = c_0\cos(\xi\,\omega_{,\xi}) - s_0\sin(\xi\,\omega_{,\xi}), \end{aligned}$$

   where $s_0 \doteq \sin\omega_0$, $c_0 \doteq \cos\omega_0$, for $\omega_0 \doteq \omega(\xi = 0)$, and the derivative $\omega_{,\xi} = \frac{1}{2}(\omega_2 - \omega_1)$. Hence,

$$\mathbf{a}_2 = c\,\mathbf{t}_2 - s\,\mathbf{t}_1 = \cos(\xi\,\omega_{,\xi})\,\mathbf{a}^0_2 - \sin(\xi\,\omega_{,\xi})\,\mathbf{a}^0_1, \tag{12.119}$$

   where $\mathbf{a}^0_2 \doteq c_0\,\mathbf{t}_2 - s_0\,\mathbf{t}_1$ and $\mathbf{a}^0_1 \doteq s_0\,\mathbf{t}_2 + c_0\,\mathbf{t}_1$.

Next, eqs. (12.118) and (12.119) are inserted into eq. (12.116).

Using the conditions (12.115), we obtain the following components of $\Delta\mathbf{u}$:

$$(\Delta\mathbf{u}\cdot\mathbf{a}^0_1) = \frac{L}{8}\,\omega_{,\xi}\left(\mathbf{t}_1 + \frac{2}{L}\mathbf{u}^0_{,\xi}\right)\cdot\mathbf{a}^0_2, \quad (\Delta\mathbf{u}\cdot\mathbf{a}^0_2) = -\frac{L}{4}\,\omega_{,\xi}\left(\mathbf{t}_1 + \frac{2}{L}\mathbf{u}^0_{,\xi}\right)\cdot\mathbf{a}^0_1, \tag{12.120}$$

and the hierarchical mid-side displacement vector can be expressed as

$$\Delta\mathbf{u} = (\Delta\mathbf{u}\cdot\mathbf{a}^0_1)\;\mathbf{a}^0_1 + (\Delta\mathbf{u}\cdot\mathbf{a}^0_2)\;\mathbf{a}^0_2. \tag{12.121}$$

Mid-side displacement vector for small strains. If we assume that strains are small, i.e. (i) $\varepsilon_{12} \approx 0$ and (ii) $\varepsilon_{11} \approx 0$, then we have

$$\mathbf{t}_1 + \frac{2}{L}\mathbf{u}^0_{,\xi} = (\mathbf{y} + \mathbf{u}^L)_{,1} = \frac{2}{L}(\mathbf{y} + \mathbf{u}^L)_{,\xi} = \frac{2}{L}\tfrac{1}{2}(\mathbf{x}_2 - \mathbf{x}_1) \overset{\text{(i)}}{\approx} \frac{2}{L}\tfrac{1}{2}L_c\,\mathbf{a}^0_1 \overset{\text{(ii)}}{\approx} \mathbf{a}^0_1, \tag{12.122}$$

where $\mathbf{u}^L \doteq M_1(\xi)\,\mathbf{u}_1 + M_2(\xi)\,\mathbf{u}_2$. Due to assumption (i), the rotated vector $\mathbf{a}^0_1$ is used instead of the vector which passes through nodes, while by (ii), the current and initial element lengths are equal, i.e. $L_c \approx L$. Because $\mathbf{a}^0_1 \cdot \mathbf{a}^0_1 = 1$ and $\mathbf{a}^0_1 \cdot \mathbf{a}^0_2 = 0$, eq. (12.120) is reduced to

$$(\Delta\mathbf{u} \cdot \mathbf{a}^0_1) \approx 0, \qquad (\Delta\mathbf{u} \cdot \mathbf{a}^0_2) \approx -\frac{L}{4}\,\omega_{,\xi}, \tag{12.123}$$

and the vector of hierarchical displacements of eq. (12.121) is

$$\Delta\mathbf{u} = -\frac{L}{4}\,\omega_{,\xi}\,\mathbf{a}^0_2 = -\frac{L}{8}\,(\omega_2 - \omega_1)\,\mathbf{a}^0_2. \tag{12.124}$$

Assuming, additionally, that the rotations are small, i.e. $\omega_0 \approx 0$, we have $c_0 \approx 1$ and $s_0 \approx 0$ and so $\mathbf{a}^0_2 \doteq c_0\,\mathbf{t}_2 - s_0\,\mathbf{t}_1 \approx \mathbf{t}_2$, i.e. the vector normal to the current boundary $\mathbf{a}^0_2$ is replaced by the vector normal to the initial element boundary $\mathbf{t}^0_2$. Thus, for small rotations, eq. (12.124) yields the classical formula

$$\Delta\mathbf{u} = -\frac{L}{4}\,\omega_{,\xi}\,\mathbf{a}^0_2 = -\frac{L}{8}\,(\omega_2 - \omega_1)\,\mathbf{t}^0_2. \tag{12.125}$$

In numerical calculations we use eq. (12.124) in the form valid for all boundaries,

$$\Delta\mathbf{u}_H \doteq -\frac{L_{JK}}{8}\,(\omega_K - \omega_J)\,\mathbf{n}_{JK}, \qquad H = 5, 6, 7, 8, \tag{12.126}$$

where $J = H - 4$, $K = \mathrm{mod}(H, 4) + 1$, and L_{JK} is the length of the boundary JK. This formula can be directly used in eq. (12.104), which then depends only on corner displacements and on corner drilling rotations.

Remark 1. Note that $\mathbf{n}_{JK}$ is the vector normal to the **current** element boundary, not to the initial one, as in eq. (12.113). Hence, $\mathbf{n}_{JK}$ is a function of nodal displacements, but we freeze this dependence and do not differentiate $\mathbf{n}_{JK}$ w.r.t. nodal displacements. The fact that $\mathbf{n}_{JK}$ is updated is similar to the co-rotational formulation.

Remark 2. The proposed generalization of the classical procedure leads to a new form of Allman shape functions, involving two components of the mid-side displacement. This new form becomes particularly simple for small strains/large rotations. Using this new form, we can exploit the Total Lagrangian description and automatic differentiation. For small rotations, the new form is reduced to the classical one.

Pure bending of Allman quadrilateral. Let us consider the question of whether the Allman shape functions are able to reproduce the analytical solution for the problem of pure bending of a square membrane. We assume that the membrane is 2×2 and the boundaries are parallel to the global basis $\{\mathbf{i}_k\}$ $(k = 1, 2)$, see Fig. 12.8.

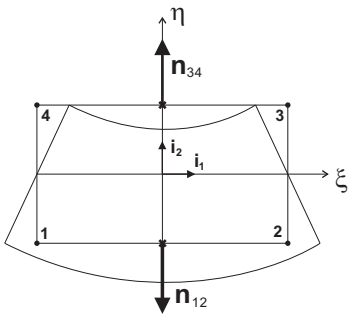

Fig. 12.8 Pure bending of the Allman quadrilateral.

First, we consider the analytical solution for pure bending of a square membrane

$$u(\xi, \eta) = A\,\xi\eta, \qquad v(\xi, \eta) = B\,(1 - \xi^2), \tag{12.127}$$

where A and B are scalar coefficients, see [98] p. 244, Fig. 4.7.2. For the analytical solution, we obtain

- the displacement gradient

$$\nabla\mathbf{u} \doteq \begin{bmatrix} u_{,\xi} & u_{,\eta} \\ v_{,\xi} & v_{,\eta} \end{bmatrix} = \begin{bmatrix} A\eta & A\xi \\ -2B\xi & 0 \end{bmatrix}, \tag{12.128}$$

- the linear strain

$$\boldsymbol{\varepsilon} \doteq \mathrm{sym}\nabla\mathbf{u} = \begin{bmatrix} u_{,\xi} & \frac{1}{2}(v_{,\xi} + u_{,\eta}) \\ \mathrm{sym.} & v_{,\eta} \end{bmatrix} = \begin{bmatrix} A\eta & \frac{1}{2}(A - 2B)\,\xi \\ \mathrm{sym.} & 0 \end{bmatrix}. \tag{12.129}$$

Next, we consider the Allman element. For pure bending, the rotations of corner nodes are as follows:

$$\omega_1 = \omega, \qquad \omega_2 = -\omega, \qquad \omega_3 = -\omega, \qquad \omega_4 = \omega \tag{12.130}$$

and the differences of rotations are

$$\omega_2 - \omega_1 = -2\,\omega, \qquad \omega_3 - \omega_2 = 0, \qquad \omega_4 - \omega_3 = 2\,\omega, \qquad \omega_1 - \omega_4 = 0.$$

From eq. (12.126) we obtain $\Delta\mathbf{u}_6 = \mathbf{0}$ and $\Delta\mathbf{u}_8 = \mathbf{0}$, i.e. the mid-side displacements for the sides which remain straight in pure bending are equal to zero. Thus, we consider only the sides which change the curvature, for which $\mathbf{n}_{12} = -\mathbf{i}_2$, $\mathbf{n}_{34} = \mathbf{i}_2$, and $L_{12} = L_{34} = 2$ and

$$\Delta\mathbf{u}_5 \doteq -\frac{L_{12}}{8}\,(\omega_2 - \omega_1)\,(\mathbf{n})_{12} = -\frac{2}{8}\,(-2\omega)\,(-\mathbf{i}_2) = -\frac{1}{2}\,\omega\,\mathbf{i}_2, \tag{12.131}$$

$$\Delta\mathbf{u}_7 \doteq -\frac{L_{34}}{8}\,(\omega_4 - \omega_3)\,(\mathbf{n})_{34} = -\frac{2}{8}\,(2\omega)\,\mathbf{i}_2 = -\frac{1}{2}\,\omega\,\mathbf{i}_2, \tag{12.132}$$

i.e. their mid-side displacements are equal, in accordance with our intuition. Substituting these expressions into eq. (12.104), we obtain the following form of the hierarchical part of displacements

$$\sum_{H=5}^{8} N_H(\xi,\eta)\;\Delta\mathbf{u}_H = N_5(\xi,\eta)\;\Delta\mathbf{u}_5 + N_7(\xi,\eta)\;\Delta\mathbf{u}_7 = v^A\,\mathbf{i}_2, \tag{12.133}$$

where $v^A(\xi) \doteq -\frac{1}{2}(1-\xi^2)\,\omega = -\frac{1}{2}M_0(\xi)\,\omega$ is the displacement component in the $\mathbf{i}_2$ direction which depends on the bubble function $M_0(\xi)$ and the drilling rotation ω. Hence, eq. (12.104) can be separately written for each component as follows:

$$u(\xi,\eta) = u_0 + \xi\,u_1 + \eta\,u_2 + \xi\eta\,u_3, \tag{12.134}$$

$$v(\xi,\eta) = v_0 + \xi\,v_1 + \eta\,v_2 + \xi\eta\,v_3 - \frac{1}{2}\underline{(1-\xi^2)\,\omega}, \tag{12.135}$$

where the contribution of $v^A(\xi)$ is underlined. For the above approximations, we obtain

- the displacement gradient

$$\nabla\mathbf{u} \doteq \begin{bmatrix} u_{,\xi} & u_{,\eta} \\ v_{,\xi} & v_{,\eta} \end{bmatrix} = \begin{bmatrix} u_1 + \eta\,u_3 & u_2 + \xi\,u_3 \\ v_1 + \eta\,v_3 + \underline{\xi\,\omega} & v_2 + \xi\,v_3 \end{bmatrix}, \tag{12.136}$$

- the linear strain

$$\boldsymbol{\varepsilon} \doteq \mathrm{sym}\nabla\mathbf{u} = \begin{bmatrix} u_{,\xi} & \frac{1}{2}(v_{,\xi} + u_{,\eta}) \\ \mathrm{sym.} & v_{,\eta} \end{bmatrix} = \begin{bmatrix} u_1 + \eta\, u_3 & \varepsilon_{12} \\ \mathrm{sym.} & v_2 + \xi\, v_3 \end{bmatrix}, \tag{12.137}$$

  where $2\varepsilon_{12} = (u_2 + v_1) + \xi\, u_3 + \eta\, v_3 + \underline{\xi\, \omega}$.

The v^A appears only in $v_{,\xi}$ and ε_{12}. Besides, the 11 and 22 components of $\nabla\mathbf{u}$ and $\boldsymbol{\varepsilon}$ are incomplete linear polynomials of ξ and η.

Remark. We can compare eqs. (12.136) and (12.137) for the Allman shape functions with eqs. (12.128) and (12.129) for the analytical solution. Concerning the displacement gradient $(\nabla\mathbf{u})_{12}$, we see that the $\xi\,\omega$ term introduced by v^A is necessary to reproduce the analytical solution. The effect of this term is similar to that of the EADG2 enhancement for the Q4 element,

$$\mathbf{G}^{\xi} = \begin{bmatrix} 0 & q_2\eta \\ q_1\xi & 0 \end{bmatrix}. \tag{12.138}$$

On the other hand, the strain representation is sufficient to reproduce the analytical solution, even without using the Allman shape functions. Nonetheless, the $\xi\omega$ term introduced into ε_{12} by the component v^A positively de-enhances it, similarly to the EADG2 enhancement. The close relation between the Allman shape functions and the EADG2 enhancement is also confirmed by numerical tests.

12.7.2 EADG2x enhancement of Allman quadrilateral

The study of a 2D beam under the in-plane shear load of Sect. 7.2.1, Table 7.1, provides a rational background for using specific enhancing strain modes for the Allman quadrilateral. The strain recovery can be interpreted as a form of strain enhancement in which we add two modes, $\{1, \zeta\}$, to the normal strain E_{33} and where $\{\varepsilon_{33}, \kappa_{33}\}$ are multipliers, see eq. (7.85). Only the recovery of κ_{33} and the ζ-mode are important for bending, which is the observation crucial for selecting proper enhancing modes for the Allman element.

The Allman element (standard, without enhancement) identically performs in the above numerical test as the beam without the κ_{33} recovery. Hence, we can enhance the Allman element using the EADG method, see Sect. 11.4.3, and the following two modes,

$$\mathbf{G}^{\xi} = \begin{bmatrix} \xi\, q_1 & 0 \\ 0 & \eta\, q_2 \end{bmatrix}, \tag{12.139}$$

designated as EADG2x. In consequence, the strain components ε_{11} and ε_{22} are enhanced, as shown below.

For simplicity, we consider a square 2×2 element, with the center located at the origin of the Cartesian coordinate system. Then the Cartesian coordinates are equal to the natural coordinates, i.e. $x = \xi$ and $y = \eta$, and the Jacobian matrix is an identity matrix. Then, for the EADG method, eq. (11.71) is reduced to $\tilde{\mathbf{H}} \doteq \mathbf{G}^{\xi}$. For eq. (11.70), the linear strain can be split into two parts

$$\mathbf{E} = \tfrac{1}{2}(\mathbf{F} + \mathbf{F}^T - 2\,\mathbf{I}) = \tfrac{1}{2}[\nabla\mathbf{u} + (\nabla\mathbf{u})^T] + \tfrac{1}{2}(\tilde{\mathbf{H}} + \tilde{\mathbf{H}}^T), \tag{12.140}$$

where the strain enhancement

$$\tfrac{1}{2}(\tilde{\mathbf{H}} + \tilde{\mathbf{H}}^T) = \begin{bmatrix} \xi\, q_1 & 0 \\ 0 & \eta\, q_2 \end{bmatrix}. \tag{12.141}$$

We see that the strain components ε_{11} and ε_{22} are indeed enhanced.

12.7.3 Special techniques for Allman quadrilateral

Even if we use the classical Allman shape functions and do not use the EADG2x enhancement, we still need to implement the two techniques which are described below.

Stabilization of spurious modes. A characteristic feature of Allman quadrilaterals are additional zero eigenvalues.

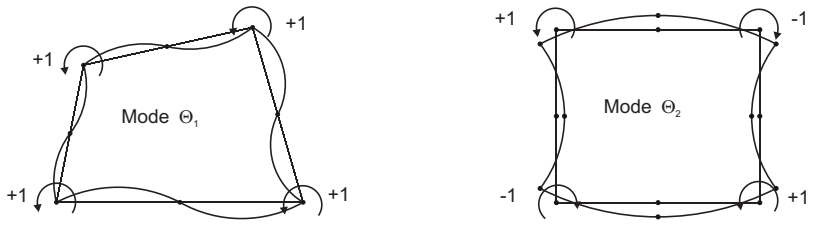

Fig. 12.9 Spurious modes Θ_1 and Θ_2 for Allman's quadrilateral.

1. If the formulation is based on the potential energy functional, then the two spurious modes shown in Fig. 12.9 are obtained. These modes can be eliminated using the penalty method and, e.g., the stabilization functions of [144],

$$P_1 = 10^{-6}\, G\, V\, \Theta_1^2, \qquad \Theta_1 \doteq \frac{1}{4}\sum_{I=1}^{4}(\omega_I - \omega_c), \quad \omega_c \doteq \tfrac{1}{2}(u_{x,y} - u_{y,x})_c, \tag{12.142}$$

$$P_2 = 10^{-3}\, G\, V\, \Theta_2^2, \qquad \Theta_2 \doteq \frac{1}{4}(\omega_1 - \omega_2 + \omega_3 - \omega_4), \tag{12.143}$$

   where ω_I are the nodal rotations and V is the element volume. Note that ω_c is identical to that obtained from the linearized drill RC equation at the element's center. It seems, however, that the form of Θ_1 should rather be $\Theta_1 \doteq \left(\frac{1}{4}\sum_{I=1}^{4}\omega_I\right) - \omega_c$.
   The tangent matrix yielded by P_2 is as follows:

$$\mathbf{K}^{\text{stab}}_{\omega\omega} = \underbrace{\frac{1}{8}10^{-3}\, G\, V}_{\text{multiplier}} \begin{bmatrix} 1 & -1 & 1 & -1 \\ -1 & 1 & -1 & 1 \\ 1 & -1 & 1 & -1 \\ -1 & 1 & -1 & 1 \end{bmatrix}. \tag{12.144}$$

   Its eigenvalues are $\{4, 0, 0, 0\} \times$ multiplier, i.e. only one eigenvalue is non-zero.
2. If the formulation is based on the functional incorporating the drill RC equation, then only one spurious mode is obtained. It is identical to Θ_2 and is eliminated by eq. (12.143). It suffices to enforce the drill RC at one point to obtain the correct rank and the center of element is a natural choice.
   Note that eq. (12.143) can be rewritten as $\Theta_2 \doteq \frac{1}{4}\mathbf{h}\cdot\boldsymbol{\omega}_I$, where $\mathbf{h} \doteq [1, -1, 1, -1]$ is the hourglass mode. After implementation of this function, the number of zero eigenvalues is three for our elements.

Adaptation of procedure of [Jetteur, Frey, 1986]. The Allman quadrilaterals have problems with passing the membrane patch test for the boundary conditions **b2** and **b3** described in Sect. 15.2.3. This problem can be circumvented by the procedure of [117]. Below, this procedure is generalized to also work for non-linear strains.

In [117], the part of membrane strains computed from the drilling rotation ω is modified as follows:

$$\tilde{\boldsymbol{\varepsilon}}(\omega) = \boldsymbol{\varepsilon}(\omega) - \frac{1}{A}\int_A \boldsymbol{\varepsilon}(\omega)\ \mathrm{d}A, \tag{12.145}$$

where $\boldsymbol{\varepsilon}(\omega)$ is the strain obtained from the hierarchical displacements

$$\mathbf{u}(\boldsymbol{\omega}_I) \doteq \sum_{H=5}^{8} N_H(\xi,\eta)\ \Delta\mathbf{u}_H \tag{12.146}$$

of eq. (12.104) and A is the element area. We see that, in eq. (12.145), the average value of $\boldsymbol{\varepsilon}(\omega)$ for the element is subtracted from $\boldsymbol{\varepsilon}(\omega)$, with the purpose of minimizing the effect of $\boldsymbol{\varepsilon}(\omega)$ on the constant strains which are checked in the patch test. Consider two cases:

- For linear strains, $\boldsymbol{\varepsilon} \doteq \mathrm{sym}\nabla\mathbf{u}$, and eq. (12.145) can be replaced by

$$\tilde{\mathbf{B}}_I\,\boldsymbol{\omega}_I = \left(\mathbf{B}_I - \frac{1}{A}\int_A \mathbf{B}_I\ \mathrm{d}A\right)\boldsymbol{\omega}_I, \tag{12.147}$$

  where $\mathbf{B}_I \doteq \partial\boldsymbol{\varepsilon}(\boldsymbol{\omega}_I)/\partial\boldsymbol{\omega}_I$, see [235], eq. (5.1)–(5.6).
- For non-linear strains, $\boldsymbol{\varepsilon}(\boldsymbol{\omega}_I)$ is complicated and therefore we replace eq. (12.145) by the formula for the gradient of the displacements depending on $\boldsymbol{\omega}_I$, i.e.

$$\widetilde{\nabla\mathbf{u}}(\boldsymbol{\omega}_I) = \nabla\mathbf{u}(\boldsymbol{\omega}_I) - \frac{1}{A}\int_A \nabla\mathbf{u}(\boldsymbol{\omega}_I)\ \mathrm{d}A, \tag{12.148}$$

  where the integral is evaluated by a 2×2 Gaussian quadrature. This formula enabled our Allman elements to pass the patch tests for the boundary conditions **b2** and **b3**, see Table 15.4.

This procedure slightly changes some of the eigenvalues but does not change the number of zero eigenvalues.

12.7.4 Allman+EADG2x elements

The Allman+EADG2x element is based on the Green strain and is valid for large drilling rotations. It uses the EADG2x enhancement and was developed using the techniques of Sect. 12.7.3. The drill RC was enforced at the element's center.

The extended functionals with drilling rotations are used to formulate two elements:

1. **Element Allman+EADG2x+P** which has the following features:
   a) the penalty method is implemented as specified in Table 12.4,
   b) it uses two additional parameters, which are multipliers of the enhancing modes.

2. **Element Allman+EADG2x+PL** which has the following features:
   a) the Perturbed Lagrange method is implemented as specified in Table 12.5. Only one parameter is used in the representation of the Lagrange multiplier of eq. (12.57), i.e. $T_a(\xi,\eta) \doteq q_0$, so eq. (12.56) becomes
   $$\mathbf{T}_a = \mathbf{J}_{Lc} \begin{bmatrix} 0 & q_0 \\ -q_0 & 0 \end{bmatrix} \mathbf{J}_{Lc}^T. \tag{12.149}$$
   b) it uses three additional parameters: two multipliers of the enhancing modes, and one parameter of the Lagrange multiplier.

These elements have a correct rank and pass the patch test for all types of boundary conditions. As indicated by the numerical results of Table 12.6, these elements have the following features: (i) their rotations converge from above, while displacements converge from below, (ii) they perform quite well for coarse distorted meshes but they are not top performers.

Finally, we note that the Allman-type 2D+drill elements can be used as the membrane part of the four-node shell element with six dofs/node. Typically, they are used in "flat" shell elements, e.g. in [3, 57], due to the lack of Allman shape functions for initially warped elements. For the latter elements, the curvature (warping) correction must be applied, as in [117, 235]; this topic is addressed in Sect. 14.

12.8 Numerical tests

Below are presented the most indicative numerical tests related to the implementation of the drilling rotation; other tests can be found in [43, 57, 56, 266, 102].

12.8.1 Comparison of various elements

All the tested 2D+drill elements have a correct rank and pass the patch test for all types of boundary conditions for the drilling rotation of Table 15.4.

Cook's membrane. The performance of 2D and 2D+drill elements is compared in Cook's membrane test, which is very demanding, see Sect. 15.2.7.

Two meshes are used in computations; a coarse 2×2-element mesh and a fine 32×32-element mesh. The regularizing parameter $\gamma = G$. The vertical displacements and the drilling rotation at point A, see Fig. 15.9, are

given in Table 12.6. The results for the penalty (P) method and the Perturbed Lagrange (PL) method are identical, which is indicated as P=PL.

We see that the best coarse mesh performance in the class of the 2D+drill elements is provided by the elements HR7-S+EADG2 and HW18-SS+EADG2. Among the elements using a small number of additional parameters, the EADG4 element is better than the HR5-S element; the converse is true for their 2D counterparts.

Table 12.6 Cook's membrane. Linear test. $\gamma = G$.

Formulation	Element	Mesh 2×2		Mesh 32×32	
		u_y	ω	u_y	ω
2D	Q4	11.845	-	23.818	-
2D+drill	Q4 (P=PL)	11.173	0.316	23.790	0.876
2D	EADG4	21.050	-	23.940	-
2D+drill	EADG4 (P=PL)	20.940	0.879	23.936	0.891
2D	HR5-S	21.353	-	23.940	-
2D+drill	HR5-S (P=PL)	18.495	0.634	23.911	0.881
2D	HR7-S+EADG2	21.353	-	23.940	-
2D+drill	HR7-S+EADG2 (P=PL)	21.263	0.899	23.936	0.890
2D	HW14-SS	21.353	-	23.940	-
2D+drill	HW14-SS (P=PL)	18.490	0.634	23.911	0.881
2D	HW18-SS	21.353	-	23.940	-
2D+drill	HW18-SS+EADG2 (P=PL)	21.237	0.895	23.936	0.891
2D+drill	Allman+EADG2x (P=PL)	20.253	1.109	23.930	0.899
Ref.		23.81		23.81	

12.8.2 Selection of the value of regularization parameter

Below, we establish the effect of the value of the regularization parameter in order to select the most suitable value for it.

In the tests we use the four-node EADG4 element with the drill RC part, in which we use the Perturbed Lagrange method with the local multipliers, implemented as described in Table 12.5, and eliminated on the element's level.

Straight cantilever beam. This test is described in Sect. 15.2.6. Here the in-plane shear load is considered and four meshes are tested, of either 6×1 or 12×2 elements, and of either rectangular or trapezoidal elements.

The vertical displacements and the drilling rotation at the end of cantilever are shown for $\gamma \in [10^0, 10^{15}]$ in Fig. 12.10 and we note a deterioration of accuracy for trapezoidal elements. For the 12×2 element mesh, the dependence on the regularization parameter γ varies. Three selected

values of this parameter, G, $G/10$, $G/100$, are marked in this figure by vertical lines. We see that $\gamma = G/100$ yields a slightly better accuracy than $\gamma = G/10$, and clearly better than $\gamma = G$.

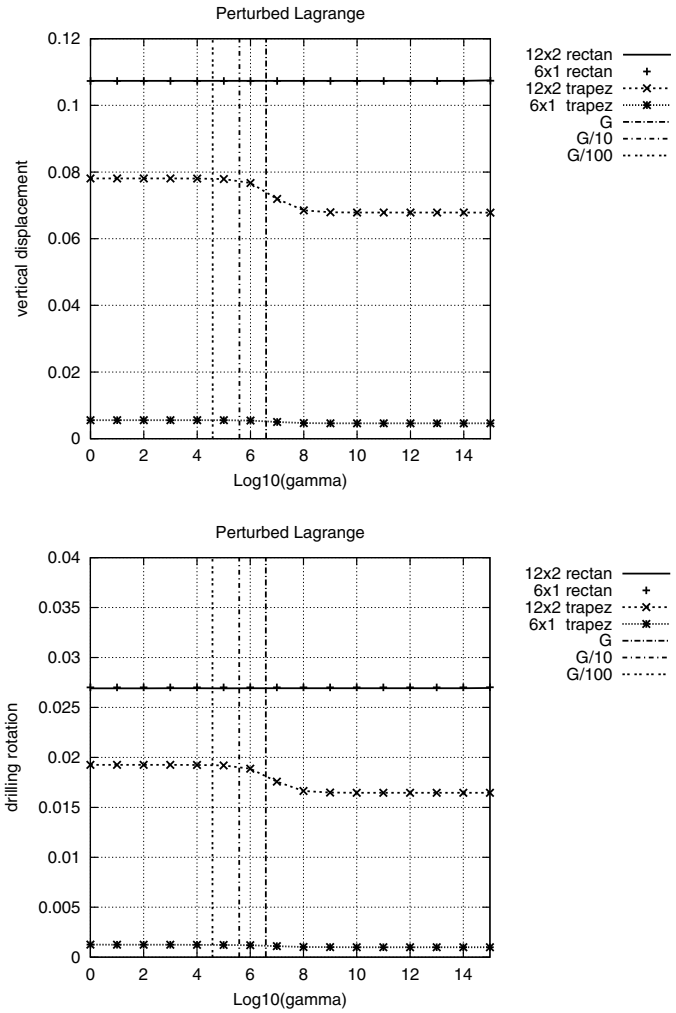

Fig. 12.10 Straight cantilever beam. Effect of γ for various shapes of elements. a) vertical displacement at point A, b) drilling rotation at point A.

Cook's membrane. In this test, elements are skew and tapered and the shear deformation dominates, see Sect. 15.2.7. Three meshes are used in

computations: 2×2, 4×4, and the fine 32×32-element mesh which is used for reference.

The vertical displacement and drill rotations are shown for $\gamma \in [10^{-10}, 10^{10}]$ in Fig. 12.11. Three selected values of γ are marked in this figure by vertical lines G, $G/10$ and $G/100$. For the displacement, the conclusion is similar to that of the previous example, i.e. $\gamma = G/100$ yields the best accuracy. For the drilling rotation, the plots are too complicated to be the basis for any conclusion.

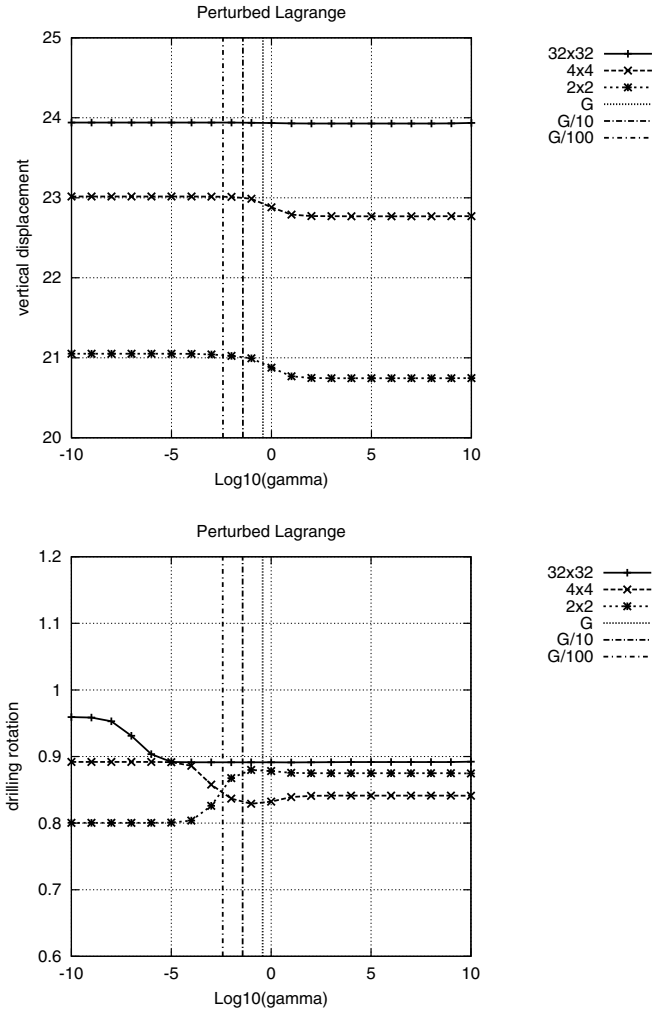

Fig. 12.11 Cook's membrane. Effect of γ for various meshes.
a) Vertical displacement at point A, b) drilling rotation at point A.

Bending of slender cantilever by end drilling rotations. This test checks whether the drilling rotation is correctly linked with displacements and transferred between elements. The drilling rotation $\omega^* = 1.2 \times 10^{-3}$ is prescribed at two tip nodes of a slender cantilever, see Fig. 12.12. The mesh consists of 1×100 elements, and the elements are 1×1 squares. The geometry and data are defined in Sect. 15.3.1.

The vertical displacements are monitored at the tip nodes where the drilling rotations are applied and they are identical for both nodes. The reference value is the Timoshenko beam solution $u_y = 0.06$. The dependence on $\gamma \in [10^0, 10^{15}]$ is shown in Fig. 12.13.

Three selected values of γ are shown in this figure by vertical lines G, $G/10$ and $G/100$. The best accuracy yields $\gamma = G$. An identical conclusion is obtained for the horizontal displacement.

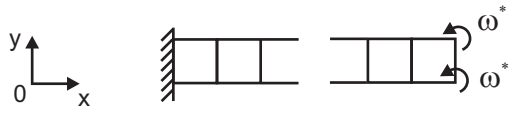

Fig. 12.12 Slender cantilever loaded by end rotations. 100 of 1×1 elements.

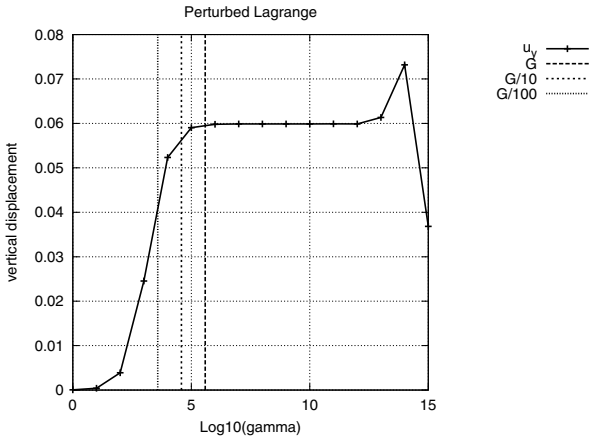

Fig. 12.13 Bending of cantilever by end drilling rotation. Effect of γ.

Conclusion. These three tests indicate that if elements are rectangular, then the value $\gamma = G$ should be used, while for the elements of distorted irregular shape the reduced value $\gamma = G/100$ seems to be optimal. Finally, we note that the reduced value of γ is also beneficial for the warped elements described in Sect. 14.